

**MICROWAVE LABORATORY REPORT NO. 89-P-1**

**MODE MATCHING ANALYSIS  
OF THE COPLANAR MICROSTRIP LINE  
ON A  
LAYERED DIELECTRIC SUBSTRATE**

**TECHNICAL REPORT**

**AFRODITI VENNIE FILIPPAS AND TATSUO ITOH**

**APRIL 1989**

**ARMY RESEARCH OFFICE  
CONTRACT DAAL03-88-K-0005**

**DTIC  
ELECTE  
JUN 16 1989**

**E D**

**THE UNIVERSITY OF TEXAS  
DEPARTMENT OF ELECTRICAL ENGINEERING  
AUSTIN, TEXAS 78712**

This document has been approved  
for public release and sale in  
distribution is unlimited.

## REPORT DOCUMENTATION PAGE

1a. REPORT SECURITY CLASSIFICATION <u>Unclassified</u>		1b. RESTRICTIVE MARKINGS	
2a. SECURITY CLASSIFICATION AUTHORITY		3. DISTRIBUTION/AVAILABILITY OF REPORT  Approved for public release; distribution unlimited.	
2b. DECLASSIFICATION/DOWNGRADING SCHEDULE			
4. PERFORMING ORGANIZATION REPORT NUMBER(S)		5. MONITORING ORGANIZATION REPORT NUMBER(S)  <u>ARO 25045-21-EL</u>	
6a. NAME OF PERFORMING ORGANIZATION  University of Texas	6b. OFFICE SYMBOL (if applicable)	7a. NAME OF MONITORING ORGANIZATION  U. S. Army Research Office	
6c. ADDRESS (City, State, and ZIP Code)  Dept. of Electrical and Comp. Engrg. AUSTIN, Texas 78712		7b. ADDRESS (City, State, and ZIP Code)  P. O. Box 12211 Research Triangle Park, NC 27709-2211	
8a. NAME OF FUNDING/SPONSORING ORGANIZATION  U. S. Army Research Office	8b. OFFICE SYMBOL (if applicable)	9. PROCUREMENT INSTRUMENT IDENTIFICATION NUMBER  <u>DAAL03-88-K-0005</u>	
8c. ADDRESS (City, State, and ZIP Code)  P. O. Box 12211 Research Triangle Park, NC 27709-2211		10. SOURCE OF FUNDING NUMBERS	
		PROGRAM ELEMENT NO	PROJECT NO
11. TITLE (Include Security Classification)  Mode matching analysis of a coplanar microstrip line on a layered dielectric substrate			
12. PERSONAL AUTHOR(S)  <u>Afroditi Vennie Filippas and Tatsuo Itoh</u>			
13a. TYPE OF REPORT  technical report	13b. TIME COVERED FROM TO	14. DATE OF REPORT (Year, Month, Day)  April 1989	15. PAGE COUNT  83
16. SUPPLEMENTARY NOTATION  The view, opinions and/or findings contained in this report are those of the author(s) and should not be construed as an official Department of the Army position, policy, or decision, unless so designated by other documentation.			
17. COSATI CODES		18. SUBJECT TERMS (Continue on reverse if necessary and identify by block number)	
FIELD	GROUP	SUB-GROUP	
19. ABSTRACT (Continue on reverse if necessary and identify by block number)  In this project, mode matching was used to calculate the propagation constant and the characteristic impedance of a coplanar coupled microstrip line. The striplines are considered to be perfect electric conductors of negligible thickness, and are separated from the ground plane by three layers of dielectric material. The layer with the higher dielectric constant is sandwiched between two layers of lower dielectric constants, such that the field is confined to this middle layer, which is called the "conducting layer" of the microstrip line. By confining the field to this layer, losses at the metal conductor are minimized.			
20. DISTRIBUTION/AVAILABILITY OF ABSTRACT <input type="checkbox"/> UNCLASSIFIED/UNLIMITED <input type="checkbox"/> SAME AS RPT. <input type="checkbox"/> DTIC USERS		21. ABSTRACT SECURITY CLASSIFICATION  Unclassified	
22a. NAME OF RESPONSIBLE INDIVIDUAL  Tatsuo Itoh		22b. TELEPHONE (Include Area Code)  (512) 471-1072	22c. OFFICE SYMBOL

**MICROWAVE LABORATORY REPORT NO. 89-P-1**

**MODE MATCHING ANALYSIS  
OF THE COPLANAR MICROSTRIP LINE  
ON A  
LAYERED DIELECTRIC SUBSTRATE**

**TECHNICAL REPORT**

**AFRODITI VENNIE FILIPPAS AND TATSUO ITOH**



**APRIL 1989**

**ARMY RESEARCH OFFICE  
CONTRACT DAAL03-88-K-0005**

Accession For	
NTIS GRA&I	<input checked="" type="checkbox"/>
DTIC TAB	<input type="checkbox"/>
Unannounced	<input type="checkbox"/>
Justification	
By	
Distribution/	
Availability Codes	
Dist	Avail and/or Special
A-1	

**THE UNIVERSITY OF TEXAS**

**DEPARTMENT OF ELECTRICAL ENGINEERING**

**AUSTIN, TEXAS 78712**

## Table of Contents

Introduction	1
Planar Transmission Media	1
Chapter 1. Mode Matching	3
Chapter 2. Analysis of the coupled microstrip line	5
2.1. Parallel-plate waveguides	5
2.2. Three-layer parallel-plate waveguide	8
2.3. Four-layer parallel-plate waveguide	17
Chapter 3. Coupled microstrip lines	22
3.1. Propagation constant	24
3.2. Characteristic Impedance	47
Chapter 4. Numerical Results	54
4.1. Convergence criteria	54
4.2. Program verification	57
4.3. Results-Design charts	59
Chapter 5. Conclusions	72
Appendix A. Notations	74
Appendix B. Field equation derivation	75
References	82

## **Introduction.**

### **Planar Transmission Media**

Planar transmission media at millimeter wavelengths provide a reasonably good performance and lend themselves to mass production techniques. There are three categories under which such lines may be placed; planar and quasi-planar (i.e. microstrip line and its variations, and finline), dielectric guides (dielectric slab, image line, insular guide, inverted image line, etc.), and H-guides (groove guide, trough guide, etc.) [14].

At millimeter wavelengths, the most commonly used planar transmission lines are microstrip and microstrip-like (inverted and suspended) lines. These lines are suitable for the design of low-cost, mass-producible millimeter wave integrated circuits. For microwave integrated circuits up to 110 GHz, the main contenders are microstrip, suspended microstrip, fin line and image line. Some examples of these lines are presented in figure 1.

Microstrip and microstrip-like transmission lines consist mainly of a thin strip conductor on a homogeneous or inhomogeneous dielectric substrate that is backed by a ground plane of infinite conductivity. Many numerical and analytical techniques exist which are used to analyze the behavior of these media [15]. One of the simplest of these methods is the quasi-static approach [6]. This approach, however, has a limited range of validity, as the nature of the mode of propagation in this case is assumed to be pure TEM, and the transmission line characteristics are calculated from the electrostatic mutual- and self capacitances and inductances of the structure. The quasi-static analysis is therefore adequate for designing circuits only when the strip

width and the substrate thickness are very small compared to the wavelength in the dielectric material.

The full-wave approach, on the other hand, is complete and rigorous. It takes into account the hybrid nature of the mode of propagation, and the transmission line characteristics are calculated by determining the propagation constant of the device. The aforementioned hybrid modes are a superposition of  $TM^y$  and  $TE^y$  fields that may, in turn, be expressed in terms of two scalar functions,  $\psi$  and  $\tilde{\psi}$ , respectively.

There are several methods available for calculating the propagation constant, including the integral equation methods, finite difference methods, spectral domain methods [2,8,18], and mode matching [7,10,11,19].

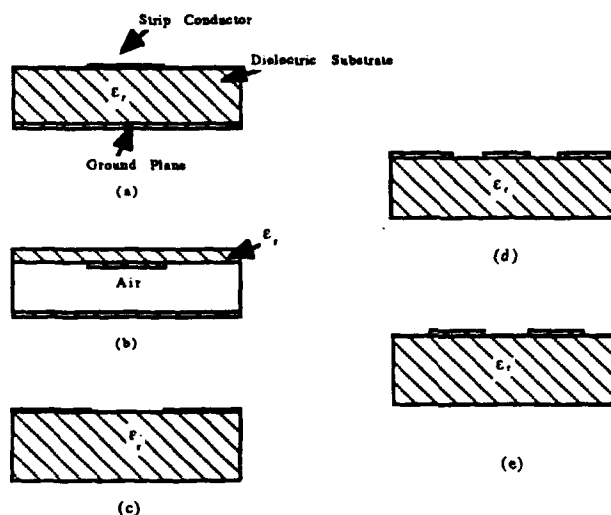


Figure 1. Some examples of planar transmission lines: (a) microstrip line, (b) inverted microstrip line, (c), (d) coplanar waveguide, and (e) coupled microstrip line.

## Chapter 1. Mode Matching.

Mode matching is one of the most frequently used techniques for formulating boundary value problems. Its primary advantage is that it does not generate spurious solutions. It does, however, have a relative convergence problem, so the accuracy of the results should be verified carefully. It is not a very efficient method, and not suitable for CAD packages, but it does afford an exact solution within a logical margin of error.

Mode matching is used when the structure in question can be identified as the junction of two or more regions, each belonging to a separable coordinate system. For a planar structure, rectangular cartesian coordinates, which are a separable system, are used to describe the structure. One other consideration in mode matching is that in each region, there must exist a set of well-defined solutions of Maxwell's equations which satisfy all the boundary conditions of the structure, except the continuity conditions at the junctions between the regions. Thus, the separation of the structure into regions must be done in a well-defined and judicious manner such that a simple and well-converging solution may be obtained.

The steps followed in the mode-matching procedure are simple and straightforward. The first step is to define a certain set of normal basis functions for each region of the device, and to expand the unknown fields in these regions with respect to these normal functions. For the sake of simplicity, these basis functions will be called "modes", although they do not satisfy the source-free wave equation with all the boundary conditions. They do, however, satisfy the wave equation in their respective regions, and they will be subject to the boundary conditions of those regions. The functional forms of these modes are already known,

so the electric fields are now actually defined by the weight of each mode. In this manner, the original problem reduces to that of determining the set of modal coefficients associated with the field expansions in the various regions. This procedure leads to an infinite set of linear simultaneous equations for the unknown modal coefficients. To obtain the exact solution to the problem at hand, one must solve this infinite set of equations, a generally impossible task. Approximation techniques, such as truncation or iteration, must therefore be applied, and herein lies the difficulty of mode matching. In a straightforward analysis, the number of modes retained will determine the accuracy of the solution. More modes would logically seem to provide a more accurate solution. However, computation time increases as the square of the number of modes retained. This is one important factor which necessarily limits the number of modes which can be retained in each region. Another source of numerical difficulties arises from the fact that planar structures such as the microstrip have geometrical discontinuities in the form of sharp edges. In this case, the fields must be subjected to one more physical condition, known as the edge condition, which states that the power of the electric and the magnetic fields at the edges must be finite. This extra condition is needed so that a unique solution to Maxwell's equations may be obtained. In mode matching, this condition translates into a relationship between the number of modes retained in each region and the actual physical dimensions of the regions. This relationship will become more clear as the analysis of the particular device under consideration, the coplanar microstrip line, progresses.

The mode matching technique may be extended to include cases of continuous spectra. This work, however, will not take such a case into consideration.



## Chapter 2. Analysis of the Coupled Microstrip Line

### 2.1. Parallel-plate Waveguides

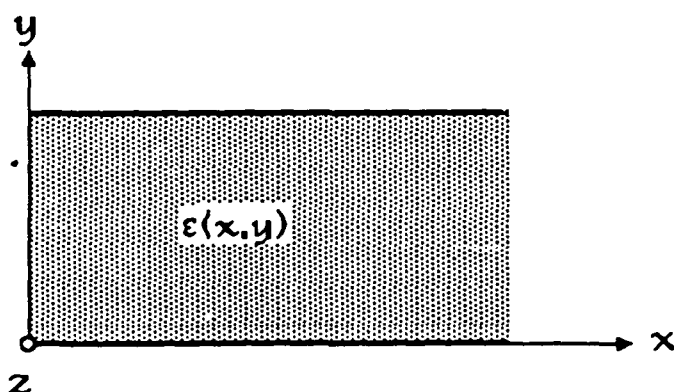


Figure 2. Parallel-plate waveguide. The medium between the plates is described by the general dielectric constant  $\epsilon(x,y)$ .

A parallel-plate waveguide (figure 2) is a rectangular structure, so it can easily be described using rectangular cartesian coordinates. Without loss of generality, it can be assumed that the metal plates of the waveguide lie parallel to the plane of two of the axes, and that the direction of propagation lies on one of these axes. The medium between the plates may be homogeneous or inhomogeneous. In the case of a homogeneous medium, finding the field distribution is elementary and the procedure may be found in any textbook. In the latter case of an inhomogeneous medium, the case where the medium is layered in only one direction, parallel to the plane of the metal plates of the waveguide, will be investigated. Assuming that the plates lie

parallel to the x-z plane, and that the direction of propagation is along the z axis, TM<sup>y</sup> and TE<sup>y</sup> solutions to Maxwell's equations may be constructed. Using untilded variables to denote TM<sup>y</sup> quantities, and tilded variables to denote TE<sup>y</sup> quantities, the TM<sup>y</sup> field components may be written as (see Appendix B) [13]:

$$\begin{aligned}
 E_x &= \frac{1}{j \omega \epsilon(y)} \frac{\partial^2 f(x,y)}{\partial x \partial y} e^{-jk_z z} & H_x &= j k_z f(x,y) e^{-jk_z z} \\
 E_y &= \frac{1}{j \omega \epsilon(y)} \left( k^2 + \frac{\partial^2}{\partial y^2} \right) f(x,y) e^{-jk_z z} & H_y &= 0 \\
 E_z &= - \frac{k_z}{\omega \epsilon(y)} \frac{\partial f(x,y)}{\partial y} e^{-jk_z z} & H_z &= \frac{\partial f(x,y)}{\partial x} e^{-jk_z z}
 \end{aligned} \tag{2.1.1}$$

where  $f(x,y)$  is the TM<sup>y</sup> scalar potential,  $\epsilon(y)$  is the y-dependent permittivity,  $k^2 = \omega^2 \mu_0 \epsilon(y)$  is the wavenumber, and  $k_z$  is the propagation constant in the z direction [4,7,19].

For the TE<sup>y</sup> field components, the corresponding equations are:

$$\begin{aligned}
 \tilde{E}_x &= -j k_z \tilde{f}(x,y) e^{-jk_z z} & \tilde{H}_x &= \frac{1}{j \omega \mu_0} \frac{\partial^2 \tilde{f}(x,y)}{\partial x \partial y} e^{-jk_z z} \\
 \tilde{E}_y &= 0 & \tilde{H}_y &= \frac{1}{j \omega \mu_0} \left( k^2 + \frac{\partial^2}{\partial y^2} \right) \tilde{f}(x,y) e^{-jk_z z} \\
 \tilde{E}_z &= - \frac{\partial \tilde{f}(x,y)}{\partial y} e^{-jk_z z} & \tilde{H}_z &= - \frac{k_z}{\omega \mu_0} \frac{\partial \tilde{f}(x,y)}{\partial x} e^{-jk_z z}
 \end{aligned} \tag{2.1.2}$$

Here,  $\tilde{f}(x,y)$  is the TE<sup>y</sup> scalar potential.

In a parallel plate waveguide with the x dimension of the waveguide very large, or for high frequencies, the potential functions for the TM<sup>y</sup> and the TE<sup>y</sup> fields may be assumed to be a function of y only. So, the TM<sup>y</sup> potential may be written as:

$$f(x,y) = \psi(y) \quad (2.1.3)$$

and the TE<sup>y</sup> potential function may be written as:

$$\tilde{f}(x,y) = \tilde{\psi}(y) \quad (2.1.4)$$

Substituting (2.1.3) into equations (2.1.1) for the TM<sup>y</sup> fields will yield:

$$\begin{aligned} E_x &= 0 & H_x &= j k_z \psi(y) e^{-jk_z z} \\ E_y &= \frac{1}{j \omega \epsilon(y)} \left( k^2 + \frac{d^2}{dy^2} \right) \psi(y) e^{-jk_z z} & H_y &= 0 \\ E_z &= -\frac{k_z}{\omega \epsilon(y)} \frac{d \psi(y)}{dy} e^{-jk_z z} & H_z &= 0 \end{aligned} \quad (2.1.5)$$

Similarly, substituting (2.1.4) into equations (2.1.2) for the TE<sup>y</sup> field components will yield:

$$\begin{aligned} \tilde{E}_x &= -j k_z \tilde{\psi}(y) e^{-jk_z z} & \tilde{H}_x &= 0 \\ \tilde{E}_y &= 0 & \tilde{H}_y &= \frac{1}{j \omega \mu_0} \left( k^2 + \frac{d^2}{dy^2} \right) \tilde{\psi}(y) e^{-jk_z z} \\ \tilde{E}_z &= 0 & \tilde{H}_z &= -\frac{k_z}{\omega \mu_0} \frac{d \tilde{\psi}(y)}{dy} e^{-jk_z z} \end{aligned} \quad (2.1.6)$$

## 2.2. Three-Layer Parallel-Plate Waveguide:

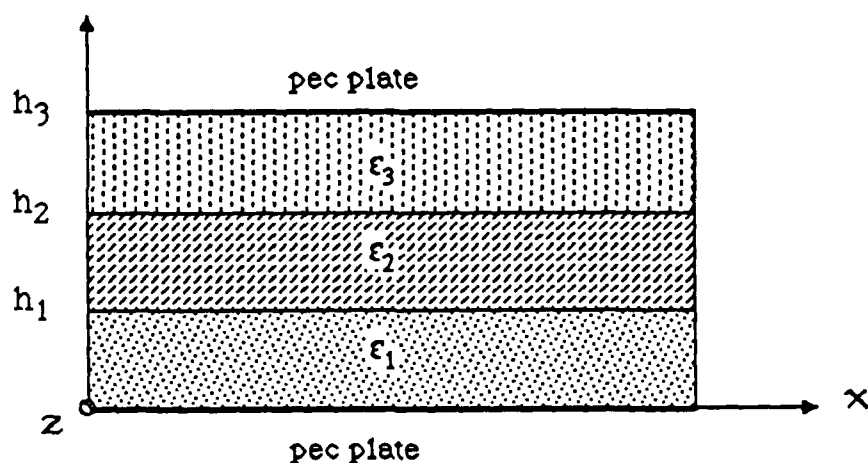


Figure 2.2.1. Three-layer parallel plate waveguide.

At this point, it would be advisable to separate the structure into regions. For a three-layer parallel-plate waveguide (a parallel plate waveguide with three layers of dielectric), the structure can be separated into three regions, each region characterized by its own dielectric. So, for the parallel-plate waveguide in fig(2.2.1), region 1 will be that region where  $0 \leq y \leq h_1$ ,  $h_1$  being the point where the dielectric constant of the medium changes from  $\epsilon_1$  to  $\epsilon_2$ . Region 2 will be that region where  $h_1 \leq y \leq h_2$ ,  $h_2$  being the point of transition from  $\epsilon = \epsilon_2$  to  $\epsilon = \epsilon_3$ . Similarly, region 3 will be that region for which  $h_2 \leq y \leq h$ ,  $h$  being the height where the top metal plate of the waveguide is situated. Each region will be characterized by its own set of  $TM^y$  and  $TE^y$  potential functions,  $f(y)$  being the  $TM^y$  potential, and  $\tilde{f}(y)$  the  $TE^y$  potential of region  $i$ ,  $i=1,2,3$ . Both the  $TM^y$  and  $TE^y$  scalar potentials are solutions of the scalar Helmholtz equation:

$$\frac{d^2 \chi(y)}{dy^2} + \kappa^2 \chi(y) = 0 \quad (2.2.1)$$

a general and complete solution to the above equation being:

$$\chi(y) = \alpha_1 \cos(\kappa y) + \alpha_2 \text{sinf}(\kappa y) \quad (2.2.2)$$

where  $\alpha_1$  and  $\alpha_2$  are constants which depend on the boundary and continuity conditions of the structure.

The function  $\text{sinf}(\kappa y)$  is defined as  $\text{sinf}(\kappa y) = \sin(\kappa y)/\kappa$  and its usefulness will be presented later on in this analysis.

The electric and magnetic fields must conform to certain boundary and continuity conditions. These conditions will serve to specify the unknown variables  $\alpha_1$ ,  $\alpha_2$ , and  $\kappa$  in equation (2.2.2). The general solution to the scalar wave equation shown above is modified such that these continuity conditions can be implemented.

Substituting  $\chi(y)$  into the  $\text{TM}^y$  equations, and applying the conditions of zero tangential electric field on the pec plates will yield the general form for the potential for the  $\text{TM}^y$  modes of a three layer parallel-plate waveguide:

$$\psi(y) = \begin{array}{ll} a \cos(k_{y1} y) & ; 0 \leq y \leq h_1 \\ b \cos[k_{y2}(h_2 - y)] \\ + c \text{sinf}[k_{y2}(h_2 - y)] & ; h_1 \leq y \leq h_2 \\ d \cos[k_{y3}(h - y)] & ; h_2 \leq y \leq h \end{array} \quad (2.2.3)$$

Correspondingly, substituting the appropriately modified forms for the corresponding form for the TE<sub>y</sub> scalar potential into the TE<sub>y</sub> field equations will yield:

$$\begin{aligned} & \tilde{a} \sin(\tilde{k}_{y1} y) && ; 0 \leq y \leq h_1 \\ \tilde{\psi}(y) = & \begin{aligned} & \tilde{b} \cos[\tilde{k}_{y2}(h_2 - y)] \\ & + \tilde{c} \sin[\tilde{k}_{y2}(h_2 - y)] \end{aligned} && ; h_1 \leq y \leq h_2 \quad (2.2.4) \\ & \tilde{d} \cos[\tilde{k}_{y3}(h - y)] && ; h_2 \leq y \leq h \end{aligned}$$

In general, the coefficients of the TM<sub>y</sub> and TE<sub>y</sub> scalar potentials, as well as their corresponding eigenvalues, will not be identically equal.

The continuity conditions between the different regions state that the tangential fields at a dielectric discontinuity must be continuous. Applying these conditions, and solving the resulting equations, will yield the eigenvalue equations for the TM<sub>y</sub> and TE<sub>y</sub> y-directed eigenvalues as well as the corresponding expansion coefficients of the scalar potentials in equations (2.2.3) and (2.2.4). The system is underdetermined, so the four expansion coefficients in each case will be found within a multiplicative constant.

Following the procedure described above will yield the TM<sub>y</sub> eigenvalue equation for the three-layer parallel-plate waveguide:

$$\begin{aligned}
& \frac{k_{y1}}{\epsilon_1} \tan(k_{y1}h_1) + \frac{k_{y2}}{\epsilon_2} \tan[k_{y2}(h_2-h_1)] + \frac{k_{y3}}{\epsilon_3} \tan[k_{y3}(h-h_2)] \\
& = \frac{k_{y1}}{\epsilon_1} \tan(k_{y1}h_1) \frac{\epsilon_2}{k_{y2}} \tan[k_{y2}(h_2-h_1)] \frac{k_{y3}}{\epsilon_3} \tan[k_{y3}(h-h_2)]
\end{aligned} \tag{2.2.5}$$

and the coefficients are:

$$d = \begin{array}{ll} 1. & k_{y3} \text{ real} \\ \frac{1.}{\cos[k_{y3}(h-h_2)]} & k_{y3} \text{ imaginary} \end{array} \tag{2.2.6.a}$$

$$c = \begin{array}{ll} -\frac{\epsilon_2}{\epsilon_3} k_{y3} \sin[k_{y3}(h-h_2)] & k_{y3} \text{ real} \\ -\frac{\epsilon_2}{\epsilon_3} k_{y3} \tan[k_{y3}(h-h_2)] & k_{y3} \text{ imaginary} \end{array} \tag{2.2.6.b}$$

$$b = \begin{array}{ll} \cos[k_{y3}(h-h_2)] & k_{y3} \text{ real} \\ 1. & k_{y3} \text{ imaginary} \end{array} \tag{2.2.6.c}$$

$$a = \frac{b \cos[k_{y2}(h_2-h_1)] + c \sin[k_{y2}(h_2-h_1)]}{\cos(k_{y1}h_1)} \tag{2.2.6.d}$$

One other relationship of great importance in this analysis is the dispersion equation. This equation links the eigenvalues  $k_x$ ,  $k_y$ , and  $k_z$ , with the wavenumber  $k$  in a certain medium. The dispersion equation states that:

$$k_x^2 + k_y^2 + k_z^2 = k^2 = \omega^2 \mu_0 \epsilon(y) \tag{2.2.7}$$

for the TM<sup>y</sup> case, and correspondingly:

$$\tilde{k}_x^2 + \tilde{k}_y^2 + k_z^2 = k^2 = \omega^2 \mu_0 \epsilon(y) \quad (2.2.8)$$

for the TE<sup>y</sup> case.

For the particular case of the three-layer parallel-plate waveguide, it has been assumed that  $k_{xi}=0$ ,  $i = 1, 2$ , and 3, so the dispersion relations for the TM<sup>y</sup> and the TE<sup>y</sup> case correspondingly become:

$$k_{yi}^2 + k_z^2 = k_i^2 = \omega^2 \mu_0 \epsilon_i \quad (2.2.9)$$

and

$$\tilde{k}_{yi}^2 + k_z^2 = k_i^2 = \omega^2 \mu_0 \epsilon_i \quad (2.2.10)$$

$k_z$  being, of course, the propagation constant of the waveguide, and  $k$  the wavenumber. The  $z$  axis (and therefore, the direction of the propagation constant) are parallel to the planes of the discontinuities, and so continuity forces  $k_z$  to be the same in every region. This gives rise to a very useful relationship between the eigenvalues in the  $y$  direction in each region. This relationship is derived by subtracting the dispersion relation defined in the one region from the corresponding equation in the other region. Thus, the dispersion relationships corresponding to two neighboring regions of the waveguide reduce to:

$$k_{yi}^2 - k_{yj}^2 = \omega^2 \mu_0 (\epsilon_i - \epsilon_j) \quad (2.2.11)$$

and:

$$\tilde{k}_{yi}^2 + \tilde{k}_{yj}^2 = \omega^2 \mu_0 (\epsilon_i - \epsilon_j) \quad (2.2.12)$$



so that the  $y$  eigenvalues in each region of the waveguide are not independent variables, but are linked through the dispersion relation.

The  $TE_y$  eigenvalue equation as well as the coefficients for the  $TE_y$  scalar potential may be derived in a manner similar to that used in the derivation of the  $TM_y$  potential. The  $TE_y$  eigenvalue equation is thus found to be:

$$\frac{\tan(\tilde{k}_{y1}h_1)}{\tilde{k}_{y1}} + \frac{\tan[\tilde{k}_{y2}(h_2-h_1)]}{\tilde{k}_{y2}} + \frac{\tan[\tilde{k}_{y3}(h-h_2)]}{\tilde{k}_{y3}} = \frac{\tan(\tilde{k}_{y1}h_1)}{\tilde{k}_{y1}} \tilde{k}_{y2} \tan[\tilde{k}_{y2}(h_2-h_1)] \frac{\tan[\tilde{k}_{y3}(h-h_2)]}{\tilde{k}_{y3}} \quad (2.2.13)$$

and the coefficients of the  $TE_y$  scalar potential in the waveguide are:

$$\tilde{d} = \begin{array}{ll} 1. & \tilde{k}_{y3} \text{ real} \\ \frac{1.}{\cos[\tilde{k}_{y3}(h-h_2)]} & \tilde{k}_{y3} \text{ imaginary} \end{array} \quad (2.2.14.a)$$

$$\tilde{c} = \begin{array}{ll} \cos[\tilde{k}_{y3}(h-h_2)] & \tilde{k}_{y3} \text{ real} \\ 1. & \tilde{k}_{y3} \text{ imaginary} \end{array} \quad (2.2.14.b)$$

$$\tilde{b} = \begin{array}{ll} \sin[\tilde{k}_{y3}(h-h_2)] & \tilde{k}_{y3} \text{ real} \\ \frac{\sin[\tilde{k}_{y3}(h-h_2)]}{\cos[\tilde{k}_{y3}(h-h_2)]} & \tilde{k}_{y3} \text{ imaginary} \end{array} \quad (2.2.14.c)$$

$$\tilde{a} = \frac{\tilde{b} \cos[\tilde{k}_{y2}(h_2-h_1)] + \tilde{c} \sin[\tilde{k}_{y2}(h_2-h_1)]}{\cos(\tilde{k}_{y1} h_1)} \quad (2.2.14.d)$$

Working in the reverse order now, the eigenvalue equation, in conjunction with the modified dispersion relation, will yield the eigenvalues in the y-direction of the three-layer parallel-plate waveguide. The dispersion relation will then yield  $k_z$ , the propagation constant of the waveguide in the z direction:

$$k_z = \sqrt{\omega^2 \mu_0 \epsilon_i - k_{yi}^2} \quad (2.2.15)$$

for the  $TM^y$  case, and

$$k_z = \sqrt{\omega^2 \mu_0 \epsilon_i - \tilde{k}_{yi}^2} \quad (2.2.16)$$

for the  $TE^y$  case.

In addition, the  $k_{yi}$  and  $\tilde{k}_{yi}$  eigenvalues serve to specify, within a multiplicative constant, the expansion coefficients of the corresponding scalar wave equations. These scalar wave equations, substituted into the corresponding  $TM^y$  or  $TE^y$  field equations will yield the  $TM^y$  or  $TE^y$  electric and magnetic field components. Since the coefficients are found only within a multiplicative constant, only the distribution of the  $\mathbf{E}$  and the  $\mathbf{H}$  fields in the waveguide can be found.

When the  $TM^y$  and  $TE^y$  scalar potentials were defined, a new functional form was introduced. This form was the function  $\text{sinf}(\kappa x)$ , which was subsequently defined as:

$$\text{sinf}(\kappa x) = \frac{\sin(\kappa x)}{\kappa} \quad (2.2.17)$$

From the definition of the "sinf" function as stated above, it is evident that this function has the following properties:

$$\frac{d}{dy} \{ \text{sinf}(\kappa x) \} = \cos(\kappa x) \quad (2.2.18)$$

and

$$\lim_{\kappa \rightarrow 0} \{ \text{sinf}(\kappa x) \} = x \quad (2.2.19)$$

The "sinf" function is preferred over the simpler "sin" because it offers two very important advantages.

One advantage is that  $\text{sinf}(\kappa x)$  offers the correct solution to the scalar Helmholtz equation for vanishing  $\kappa$ . Using sin, the general solution to the scalar wave equation is:

$$\chi(y) = \alpha_1 \cos(\kappa y) + \alpha_2 \sin(\kappa y) \quad (2.2.20)$$

As  $\kappa$  approaches 0,  $\chi(y)$  becomes:

$$\chi(y) = \alpha_1 \quad (2.2.21)$$

Although this does provide a solution, it is not a general solution to Laplace's equation.

With the "sinf" representation, however, the solution to Laplace's equation becomes:

$$\chi(y) = \alpha_1 \cos(\kappa y) + \alpha_2 \text{sinf}(\kappa y) \quad (2.2.22)$$

which, for vanishing  $\kappa$  yields:

$$\chi(y) = \alpha_1 + \alpha_2 y \quad (2.2.23)$$

This latter form does provide a general solution to Laplace's equation.

The second very important advantage of the "sinf" function over the "sin" is found in the nature of the eigenvalues  $\kappa$ . For a purely lossless dielectric medium,  $\kappa$  will be either real or imaginary. For  $\kappa$  imaginary, the "sin" function would also be imaginary, which fact might give rise to a complex analysis. However, the "sinf" function remains real irrespective of whether  $\kappa$  is real or imaginary. This provides a distinct improvement over the "sin".

For programming purposes, "sinf" is defined as:

$$\text{sinf}(\kappa x) = x * \left\{ \begin{array}{ll} 1. - \frac{(\kappa x)^2}{6.} + \frac{(\kappa x)^2}{120.} & |\kappa x| \leq 0.1 \\ \frac{\sin(\kappa x)}{\kappa x} & |\kappa x| > 0.1 \end{array} \right\} \quad (2.2.4)$$

Here, the asymptotic expression for "sinf" is used for the case  $|\kappa x| \leq 0.1$ .

### 2.3. Four-layer parallel-plate waveguide:

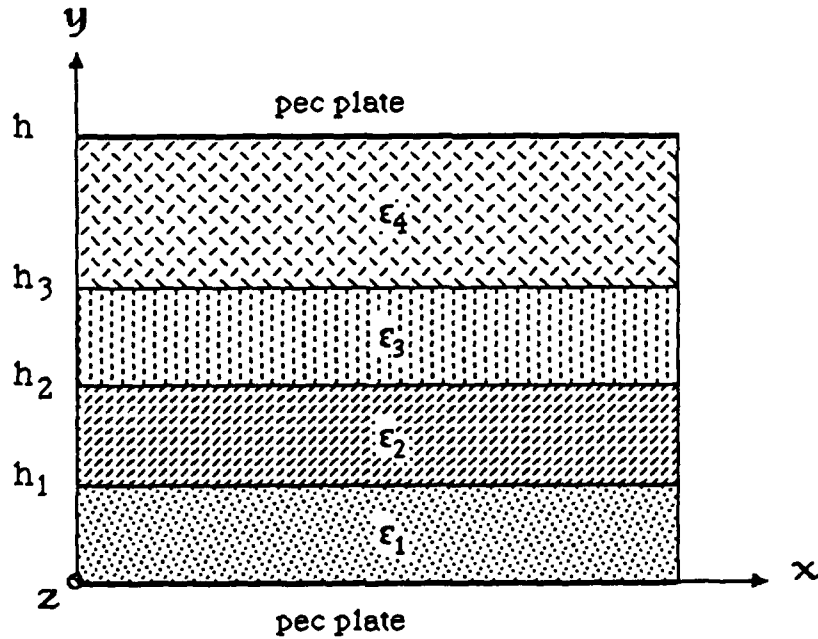


Figure 2.3.1. Four layer parallel-plate waveguide.

The  $TM^y$  scalar potential for the case of the four-layer parallel-plate waveguide may be written as:

$$\psi(y) = \begin{aligned} & a \cos(k_{y1}y) && ; 0 \leq y \leq h_1 \\ & b \cos[k_{y2}(h_2 - y)] \\ & + c \sin[k_{y2}(h_2 - y)] && ; h_1 \leq y \leq h_2 \\ & d \cos[k_{y3}(h_3 - y)] \\ & + e \sin[k_{y3}(h_3 - y)] && ; h_2 \leq y \leq h_3 \\ & f \cos[k_{y4}(h - y)] && ; h_3 \leq y \leq h \end{aligned} \quad (2.3.1)$$

The eigenvalue equation is found using the same procedure that was described for the three-layer parallel-plate waveguide. The  $TM^y$  eigenvalue equation is therefore:

$$\begin{aligned}
 & \frac{k_{y1}}{\epsilon_1} \tan(k_{y1}h_1) + \frac{k_{y2}}{\epsilon_2} \tan[k_{y2}(h_2-h_1)] \\
 & + \frac{k_{y3}}{\epsilon_3} \tan[k_{y3}(h_3-h_2)] + \frac{k_{y4}}{\epsilon_4} \tan[k_{y4}(h-h_3)] = \\
 & \frac{k_{y1}}{\epsilon_1} \tan(k_{y1}h_1) \frac{\epsilon_2}{k_{y2}} \tan[k_{y2}(h_2-h_1)] \frac{k_{y3}}{\epsilon_3} \tan[k_{y3}(h_3-h_2)] + \\
 & \frac{k_{y1}}{\epsilon_1} \tan(k_{y1}h_1) \frac{\epsilon_2}{k_{y2}} \tan[k_{y2}(h_2-h_1)] \frac{k_{y4}}{\epsilon_4} \tan[k_{y4}(h-h_3)] + \\
 & \frac{k_{y1}}{\epsilon_1} \tan(k_{y1}h_1) \frac{\epsilon_3}{k_{y3}} \tan[k_{y3}(h_3-h_2)] \frac{k_{y4}}{\epsilon_4} \tan[k_{y4}(h-h_3)] + \\
 & \frac{k_{y2}}{\epsilon_2} \tan[k_{y2}(h_2-h_1)] \frac{\epsilon_3}{k_{y3}} \tan[k_{y3}(h_3-h_2)] \frac{k_{y4}}{\epsilon_4} \tan[k_{y4}(h-h_3)]
 \end{aligned} \tag{2.3.2}$$

The coefficients which serve to define the  $TM^y$  scalar potential of the waveguide are, within a multiplicative constant:

$$\begin{aligned}
 f &= \begin{aligned} & 1. & ; k_{y4} \text{ real} \\ & \frac{1.}{\cos[k_{y4}(h-h_3)]} & ; k_{y4} \text{ imaginary} \end{aligned}
 \end{aligned} \tag{2.3.3.a}$$

$$\begin{aligned}
 e &= \begin{aligned} & -\frac{\epsilon_3}{\epsilon_2} k_{y4} \sin[k_{y4}(h-h_3)] & ; k_{y4} \text{ real} \\ & -\frac{\epsilon_3}{\epsilon_2} k_{y4} \tan[k_{y4}(h-h_3)] & ; k_{y4} \text{ imaginary} \end{aligned}
 \end{aligned} \tag{2.3.3.b}$$

$$\begin{aligned}
 d &= \begin{aligned} & \cos[k_{y4}(h-h_3)] & ; k_{y4} \text{ real} \\ & 1. & ; k_{y4} \text{ imaginary} \end{aligned}
 \end{aligned} \tag{2.3.3.c}$$

$$c = d \cos[k_{y3}(h_3 - h_2)] + e \sin[k_{y3}(h_3 - h_2)] \quad (2.3.3.d)$$

$$b = -d \frac{\epsilon_2}{\epsilon_3} k_{y3} \sin[k_{y3}(h_3 - h_2)] + e \frac{\epsilon_2}{\epsilon_3} \cos[k_{y3}(h_3 - h_2)] \quad (2.3.3.e)$$

$$a = \frac{b \cos[k_{y2}(h_2 - h_1)] + c \sin[k_{y2}(h_2 - h_1)]}{\cos(k_{y1}h_1)} \quad (2.3.3.f)$$

The TE<sup>y</sup> scalar potential may be written as:

$$\begin{aligned} \tilde{\psi}(y) = & \begin{aligned} & \tilde{a} \cos(\tilde{k}_{y1}y) && ; 0 \leq y \leq h_1 \\ & \tilde{b} \cos[\tilde{k}_{y2}(h_2 - y)] \\ & + \tilde{c} \sin[\tilde{k}_{y2}(h_2 - y)] && ; h_1 \leq y \leq h_2 \\ & \tilde{d} \cos[\tilde{k}_{y3}(h_3 - y)] \\ & + e \sin[\tilde{k}_{y3}(h_3 - y)] && ; h_2 \leq y \leq h_3 \\ & \tilde{f} \cos[\tilde{k}_{y4}(h - y)] && ; h_3 \leq y \leq h \end{aligned} \end{aligned} \quad (2.3.4)$$

Using this expression for the potential, the eigenvalue equation is found to be:

$$\begin{aligned}
& \frac{\tan(\tilde{k}_{y1}h_1)}{\tilde{k}_{y1}} + \frac{\tan[\tilde{k}_{y2}(h_2-h_1)]}{\tilde{k}_{y2}} \\
& + \frac{\tan[\tilde{k}_{y3}(h_3-h_2)]}{\tilde{k}_{y3}} + \frac{\tan[\tilde{k}_{y4}(h-h_3)]}{\tilde{k}_{y4}} = \\
& \frac{\tan(\tilde{k}_{y1}h_1)}{\tilde{k}_{y1}} \tilde{k}_{y2} \tan[\tilde{k}_{y2}(h_2-h_1)] \frac{\tan[\tilde{k}_{y3}(h_3-h_2)]}{\tilde{k}_{y3}} + \\
& \frac{\tan(\tilde{k}_{y1}h_1)}{\tilde{k}_{y1}} \tilde{k}_{y2} \tan[\tilde{k}_{y2}(h_2-h_1)] \frac{\tan[\tilde{k}_{y4}(h-h_3)]}{\tilde{k}_{y4}} + \\
& \frac{\tan(\tilde{k}_{y1}h_1)}{\tilde{k}_{y1}} \tilde{k}_{y3} \tan[\tilde{k}_{y3}(h_2-h_1)] \frac{\tan[\tilde{k}_{y4}(h-h_3)]}{\tilde{k}_{y4}} + \\
& \frac{\tan[\tilde{k}_{y2}(h_2-h_1)]}{\tilde{k}_{y2}} \tilde{k}_{y3} \tan[\tilde{k}_{y3}(h_2-h_1)] \frac{\tan[\tilde{k}_{y4}(h-h_3)]}{\tilde{k}_{y4}}
\end{aligned} \tag{2.3.5}$$

The coefficients of the scalar potential are, within a multiplicative constant:

$$\begin{aligned}
& 1. \quad ; \tilde{k}_{y4} \text{ real} \\
\tilde{f} = & \frac{1.}{\cos[\tilde{k}_{y4}(h-h_3)]} ; \tilde{k}_{y4} \text{ imaginary}
\end{aligned} \tag{2.3.6.a}$$

$$\begin{aligned}
& \cos[\tilde{k}_{y4}(h-h_3)] ; \tilde{k}_{y4} \text{ real} \\
\tilde{e} = & 1. ; \tilde{k}_{y4} \text{ imaginary}
\end{aligned} \tag{2.3.6.b}$$

$$\begin{aligned}
& \sin[\tilde{k}_{y4}(h-h_3)] ; \tilde{k}_{y4} \text{ real} \\
\tilde{d} = & \tan[\tilde{k}_{y4}(h-h_3)] ; \tilde{k}_{y4} \text{ imaginary}
\end{aligned} \tag{2.3.6.c}$$

$$\tilde{b} = \tilde{d} \cos[\tilde{k}_{y3}(h_3-h_2)] + \tilde{e} \sin[\tilde{k}_{y3}(h_3-h_2)] \tag{2.3.6.d}$$



$$\tilde{c} = -d \tilde{k}_{y3} \sin[k_{y3}(h_3-h_2)] + e \cos[\tilde{k}_{y3}(h_3-h_2)] \quad (2.3.6.e)$$

$$\tilde{a} = \frac{\tilde{b} \cos[\tilde{k}_{y2}(h_2-h_1)] + \tilde{c} \sin[\tilde{k}_{y2}(h_2-h_1)]}{\cos(\tilde{k}_{y1}h_1)} \quad (2.3.6.f)$$

Thus, so far, the  $TM^y$  and  $TE^y$  potential functions for the three- and four-layer parallel-plate waveguides have been derived. Their connection with the coupled microstrip line, which is the main subject of this paper, will become apparent shortly.

### Chapter 3. Coupled Microstrip Lines

Coupled microstrip lines are used in a number of circuit applications, principally as directional couplers, filters, and delay lines. Mode matching will be used to calculate the propagation constant of such a line.

A pair of microstrip-like transmission lines as shown in fig. (3.1) are known to have the property of a broadband directional coupler when placed in parallel proximity to each other. As a result of this proximity, a fraction of the power present on the main line is coupled to the secondary line. The power coupled is a function of the physical dimensions of the structure and the direction of propagation of the primary power.

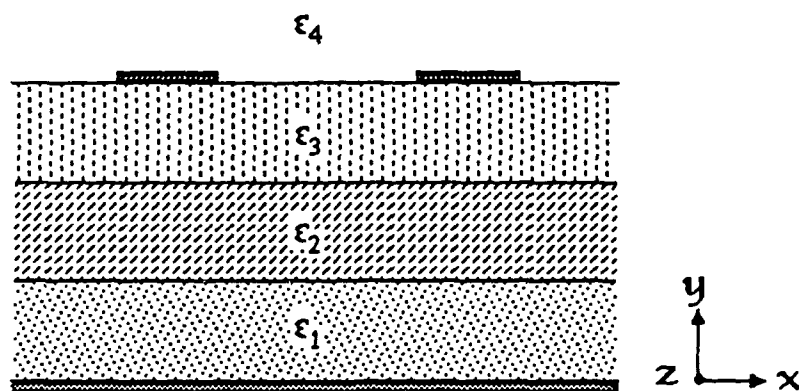


Figure 3.1. The coupled microstrip line.

In general, the coupled line structures shown in fig. (3.1) support two modes, the even and the odd modes. This induces the coupling between the two transmission lines. The properties of the coupled structures may be described in terms of a suitable linear combination of these even and odd modes. For

geometrically symmetric structures, the geometrical plane of symmetry may also be thought of as an electrical plane of symmetry. The even mode has equal amplitude and equal phase correspondence with respect to this plane of symmetry, in which case this plane takes the form of an open circuit. In the even mode case, therefore, the plane of symmetry takes the form of a perfect magnetic wall (pmc). The odd mode, on the other hand, has an equal amplitude  $180^\circ$ -out-of-phase correspondence with respect to the plane of symmetry, so this plane acts like a short circuit and is simulated by a perfect electric conductor (pec) wall. Thus, the directional coupler can be treated as a two-port network, and the total response can be obtained by superimposing the responses calculated for the even and odd mode excitations. This reduces the problem to about half its original size, which is a great advantage of symmetric structures.

### 3.1. Propagation Constant

The structure shown in figure (3.1) is symmetric with respect to a plane drawn perpendicular to the x-y and x-z planes and placed halfway between the two metal strips. Thus, the structure under consideration is modified to that shown in figure (3.1.1).

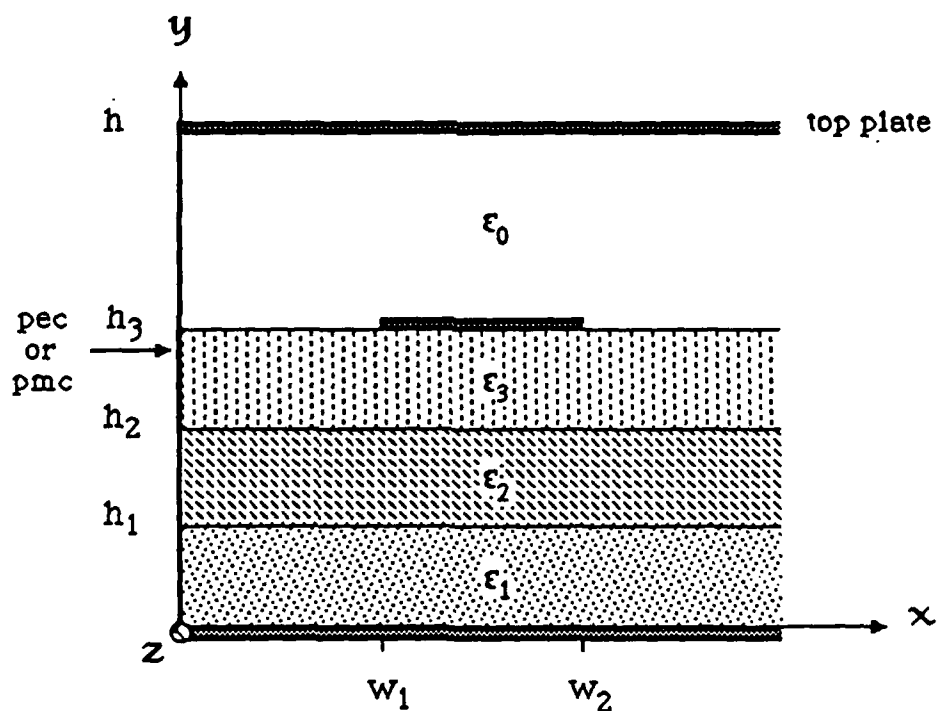


Figure 3.1.1. Symmetry as applied to the coupled microstrip line

As was mentioned earlier, the left-most boundary becomes either a pmc or a pec wall, according to whether the search is conducted for the odd-mode or even-mode propagation

constant. There is no perpendicular boundary to the right of the microstrip, so propagation in the positive  $x$  direction for large  $x$  must take the form  $\exp(-jk_x x)$ , such that there is an exponential decay for  $x \rightarrow \infty$ . This serves to put a lower bound on the search for  $k_z$ , since this exponential decay is observed only for the case where  $k_x$  is imaginary. The dispersion relation states that:

$$k_x^2 + k_y^2 + k_z^2 = k^2 = \omega^2 \mu_0 \epsilon \quad (3.1.1)$$

so, for  $k_x$ :

$$k_x^2 = \omega^2 \mu_0 \epsilon - k_y^2 - k_z^2 \quad (3.1.2)$$

The condition for imaginary  $k_x$  yields:

$$\omega^2 \mu_0 \epsilon - k_y^2 - k_z^2 < 0 \quad (3.1.3)$$

or:

$$k_z > \sqrt{\omega^2 \mu_0 \epsilon - k_y^2} \quad (3.1.4)$$

An upper bound may also be placed on  $k_z$ , since it may never be larger than the unbounded propagation constant in the medium with the highest relative dielectric constant. Thus:

$$k_z < \omega \sqrt{\mu_0 \epsilon_0 \max(\epsilon_i)} \quad (3.1.5)$$

The structure must further be separated into regions for modal expansion. Two more bounding planes may be drawn parallel to the plane of symmetry, at each end of the metal strip. Also, since the structure must be bounded, a top plate must be placed above the structure at such a distance that it does not interfere with the computation of the propagation constant of the actual open structure (this top plate was also included in figure

3.1.1). The two lateral bounding planes may be thought of as perfect magnetic conductor walls, since the tangential electric and magnetic fields must be continuous across them. The original structure has thus been separated into four distinct regions, shown in figure (3.1.2).

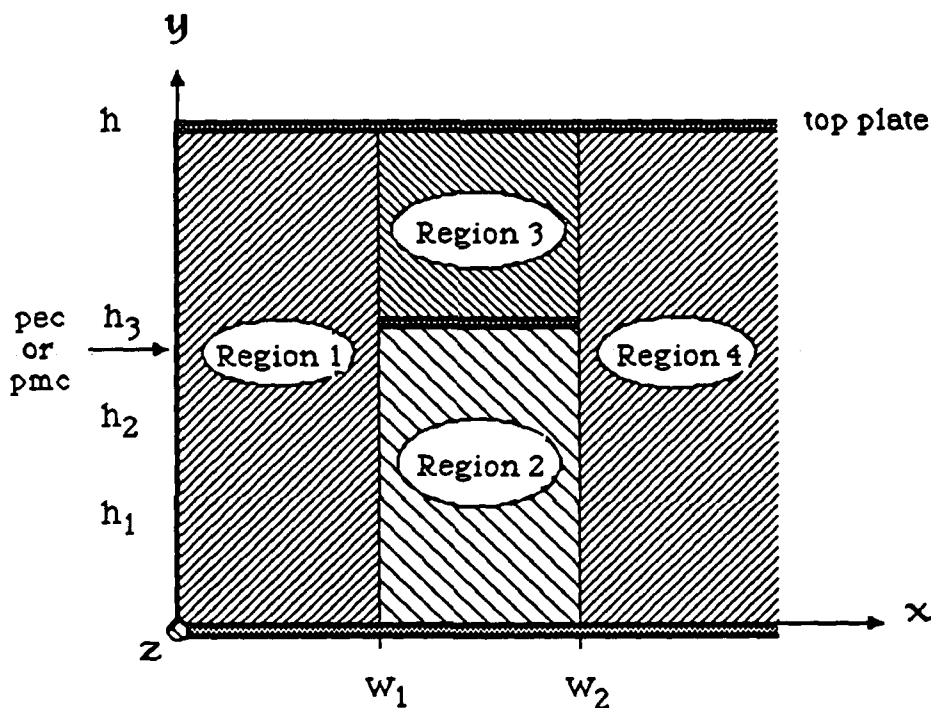


Figure 3.1.2. The four distinct regions of the coupled microstrip line

As was stated earlier, a set of normal modes must be defined for each region, and the unknown fields in each must be expanded with respect to these modes. Each region may be thought of as a multilayered parallel-plate waveguide, consisting of two parallel metal sheets placed at a certain distance from, and parallel to, each other, with a layered dielectric medium between them. Thus, regions 1 and 4 are four-layered parallel-plate

waveguides, region 2 is a three-layered parallel-plate waveguide, and region 3 is a one-layered parallel-plate waveguide. This latter case has been studied extensively in the literature, and has not been presented here. The normal modes for the three- and four-layered parallel-plate waveguides have been defined in chapters 2.2 and 2.3, respectively. It now remains to establish the equations which define the electric field components with respect to these modes. Let it be noted that the following modal expansions and field representations are not unique, but just constitute one possible solution.

Using the expressions derived for the  $TM^y$  and  $TE^y$  modes of the three- and four-layer parallel-plate waveguides, the corresponding expressions for the electric and magnetic field expansions may be derived. As shown in Appendix B, the electric and magnetic fields in each region due to the  $TM^y$  mode potentials are given by:

$$\begin{aligned}
 E_{xi} &= \frac{1}{\hat{y}_i} \frac{\partial^2 (f_i(x,y)e^{-jkz})}{\partial x \partial y} & H_{xi} &= - \frac{\partial (f_i(x,y)e^{-jkz})}{\partial z} \\
 E_{yi} &= \frac{1}{\hat{y}_i} \left( \frac{\partial^2}{\partial x^2} + k_i^2 \right) (f_i(x,y)e^{-jkz}) & H_{yi} &= 0 \\
 E_{zi} &= \frac{1}{\hat{y}_i} \frac{\partial^2 (f_i(x,y)e^{-jkz})}{\partial y \partial z} & H_{zi} &= - \frac{\partial (f_i(x,y)e^{-jkz})}{\partial x}
 \end{aligned} \tag{3.1.6}$$

and the electric and magnetic fields due to the  $TM^y$  fields are:

$$\begin{aligned}
\tilde{E}_{xi} &= \frac{\partial(\tilde{f}_i(x,y)e^{-jkz})}{\partial z} & \tilde{H}_{xi} &= \frac{1}{\hat{z}} \frac{\partial^2(\tilde{f}_i(x,y)e^{-jkz})}{\partial x \partial y} \\
\tilde{E}_{yi} &= 0 & \tilde{H}_{yi} &= \frac{1}{\hat{z}} \left( \frac{\partial^2}{\partial x^2} + k_i^2 \right) (\tilde{f}_i(x,y)e^{-jkz}) \quad (3.1.7) \\
\tilde{E}_{zi} &= -\frac{\partial(\tilde{f}_i(x,y)e^{-jkz})}{\partial x} & \tilde{H}_{zi} &= \frac{1}{\hat{z}} \frac{\partial^2(\tilde{f}_i(x,y)e^{-jkz})}{\partial y \partial z}
\end{aligned}$$

where  $\hat{y}_i = j\omega\epsilon_i$  and  $\hat{z} = j\omega\mu_0$  [13], and subscript  $i=1,2,3$ , or 4, correspondingly, for each region.



The electric and magnetic potentials in each region are:

Region 1:

$$\begin{aligned} f_{1m}(x,y) &= A_{1m} \psi_{1m}(y) \begin{matrix} \cos \\ \sin \end{matrix} (k_{1xm}x) \begin{matrix} \text{odd} \\ \text{even} \end{matrix} \\ \tilde{f}_{1m}(x,y) &= \tilde{A}_{1m} \psi_{1m}(y) \begin{matrix} \sin \\ \cos \end{matrix} (\tilde{k}_{1xm}x) \begin{matrix} \text{odd} \\ \text{even} \end{matrix} \end{aligned} \quad (3.1.8.a)$$

Region 2:

$$\begin{aligned} f_{2m}(x,y) &= \psi_{2m}^*(y) \{ A_{2m} \cos[k_{x2m}(x-w_1)] \\ &\quad + B_{2m} \sin[k_{x2m}(x-w_1)] \} \\ \tilde{f}_{2m}(x,y) &= \tilde{\psi}_{2m}(y) \{ \tilde{A}_{2m} \cos[\tilde{k}_{x2m}(x-w_1)] \\ &\quad + \tilde{B}_{2m} \sin[\tilde{k}_{x2m}(x-w_1)] \} \end{aligned} \quad (3.1.8.b)$$

Region 3:

$$\begin{aligned} f_{3m}(x,y) &= \psi_{3m}(y) \{ A_{3m} \cos[k_{x3m}(x-w_1)] \\ &\quad + B_{3m} \sin[k_{x3m}(x-w_1)] \} \\ \tilde{f}_{3m}(x,y) &= \tilde{\psi}_{3m}(y) \{ \tilde{A}_{3m} \cos[\tilde{k}_{x3m}(x-w_1)] \\ &\quad + \tilde{B}_{3m} \sin[\tilde{k}_{x3m}(x-w_1)] \} \end{aligned} \quad (3.1.8.c)$$

Region 4:

$$\begin{aligned} f_{4m}(x,y) &= \psi_{4m}(y) \exp[-jk_{4xm}(x-w_2)] \\ \tilde{f}_{4m}(x,y) &= \tilde{\psi}_{4m}(y) \exp[-j\tilde{k}_{4xm}(x-w_2)] \end{aligned} \quad (3.1.8.d)$$

where  $\psi_i(y)$  and  $\tilde{\psi}_i(y)$  are the TM<sup>y</sup> and TE<sup>y</sup> potential functions for the corresponding cases of the one-, three-, and four-layer parallel-plate waveguides.

For a suppressed  $z$ -dependence, the equations for the electric and magnetic field components yield, for each region:

## REGION 1

Electric Field Components:

$$E_{1x} = \frac{1}{j\omega\epsilon_1(y)} \sum_{m=1}^{M_1} \frac{d\psi_{1m}(y)}{dy} \begin{pmatrix} -k_{1xm} \\ 1 \end{pmatrix} \frac{\sin(k_{1xm}x)}{\cos(k_{1xm}x)} A_{1m} \\ - jk_z \sum_{m=1}^{M_1} \tilde{\psi}_{1m}(y) \frac{\sin(\tilde{k}_{1xm}x)}{\cos(\tilde{k}_{1xm}x)} \tilde{A}_{1m}$$

$$E_{1y} = \frac{1}{j\omega\epsilon_1(y)} \sum_{m=1}^{M_1} (k_z^2 + k_{1xm}^2) \psi_{1m}(y) \frac{\cos(k_{1xm}x)}{\sin(k_{1xm}x)} A_{1m} \quad (3.1.9.a)$$

$$E_{1z} = - \frac{1}{j\omega\epsilon_1(y)} \sum_{m=1}^{M_1} \frac{d\psi_{1m}(y)}{dy} \frac{\cos(k_{1xm}x)}{\sin(k_{1xm}x)} A_{1m} \\ - \sum_{m=1}^{M_1} \tilde{\psi}_{1m}(y) \begin{pmatrix} 1 \\ -k_{1xm} \end{pmatrix} \frac{\cos(\tilde{k}_{1xm}x)}{\sin(\tilde{k}_{1xm}x)} \tilde{A}_{1m}$$

Magnetic Field Components:

$$H_{1x} = jk_z \sum_{m=1}^{M_1} \psi_{1m}(y) \frac{\cos(k_{1xm}x)}{\sin(k_{1xm}x)} A_{1m} \\ + \frac{1}{j\omega\mu_0} \sum_{m=1}^{M_1} \frac{d\tilde{\psi}_{1m}(y)}{dy} \begin{pmatrix} 1 \\ -\tilde{k}_{1xm} \end{pmatrix} \frac{\cos(\tilde{k}_{1xm}x)}{\sin(\tilde{k}_{1xm}x)} \tilde{A}_{1m}$$

(3.1.9.b)

$$H_{1y} = \frac{1}{j\omega\mu_0} \sum_{m=1}^{M_1} (k_z^2 + \tilde{k}_{1xm}^2) \tilde{\psi}_{1m}(y) \frac{\sin(\tilde{k}_{1xm}x)}{\cos(\tilde{k}_{1xm}x)} \tilde{A}_{1m}$$

$$H_{1z} = \sum_{m=1}^{M_1} \psi_{1m}(y) \begin{pmatrix} -k_{1xm} \\ 1 \end{pmatrix} \frac{\sin(k_{1xm}x)}{\cos(k_{1xm}x)} A_{1m} \\ - \frac{k_z}{\omega\mu_0} \sum_{m=1}^{M_1} \frac{d\tilde{\psi}_{1m}(y)}{dy} \frac{\sin(\tilde{k}_{1xm}x)}{\cos(\tilde{k}_{1xm}x)} \tilde{A}_{1m}$$

## REGION 2

Electric Field Components:

$$\begin{aligned}
E_{2x} = & \frac{1}{j\omega\epsilon_2(y)} \sum_{m=1}^{M_2} \frac{d\psi_{2m}(y)}{dy} \{ -A_{2m}k_{2xm}\sin[(k_{2xm}(x-w_1)] \\
& + B_{2m}\cos[(k_{2xm}(x-w_1))] \} + \\
& jk_z \sum_{m=1}^{M_2} \tilde{\psi}_{2m}(y) \{ \tilde{A}_{2m}\cos[\tilde{k}_{2xm}(x-w_1)] \\
& + \tilde{B}_{2m}\sin[\tilde{k}_{2xm}(x-w_1)] \} \\
E_{2y} = & \frac{1}{j\omega\epsilon_2(y)} \sum_{m=1}^{M_2} (k_z^2 + k_{2xm}^2) \psi_{2m}(y) \{ A_{2m}\cos[(k_{2xm}(x-w_1)] \\
& + B_{2m}\sin[(k_{2xm}(x-w_1))] \} \\
E_{2z} = & -\frac{k_z}{\omega\epsilon_2(y)} \sum_{m=1}^{M_2} \frac{d\psi_{2m}(y)}{dy} \{ A_{2m}\cos[(k_{2xm}(x-w_1)] \\
& + B_{2m}\sin[(k_{2xm}(x-w_1))] \} - \\
& \sum_{m=1}^{M_2} \tilde{\psi}_{2m}(y) \{ -\tilde{A}_{2m}\tilde{k}_{2xm}\sin[\tilde{k}_{2xm}(x-w_1)] \\
& + \tilde{B}_{2m}\cos[\tilde{k}_{2xm}(x-w_1)] \}
\end{aligned} \tag{3.1.10.a}$$

Magnetic Field Components:

$$\begin{aligned}
 H_{2x} = & jk_z \sum_{m=1}^{M_1} \psi_{1m}(y) \{ A_{2m} \cos[k_{2xm}(x-w_1)] \\
 & + B_{2m} \sin[k_{2xm}(x-w_1)] \} + \\
 & \frac{1}{j\omega\mu_0} \sum_{m=1}^{M_2} \frac{d\tilde{\psi}_{2m}(y)}{dy} \{ -\tilde{A}_{2m} \tilde{k}_{2xm} \cos[\tilde{k}_{2xm}(x-w_1)] \\
 & + \tilde{B}_{2m} \sin[\tilde{k}_{2xm}(x-w_1)] \} \quad (3.1.10.b)
 \end{aligned}$$

$$\begin{aligned}
 H_{2y} = & \frac{1}{j\omega\mu_0} \sum_{m=1}^{M_2} (k_z^2 + \tilde{k}_{2xm}^2) \tilde{\psi}_{2m}(y) \{ \tilde{A}_{2m} \cos[\tilde{k}_{2xm}(x-w_1)] \\
 & + \tilde{B}_{2m} \sin[\tilde{k}_{2xm}(x-w_1)] \}
 \end{aligned}$$

$$\begin{aligned}
 H_{2z} = & \sum_{m=1}^{M_2} \psi_{2m}(y) \{ -A_{2m} k_{2xm} \sin[k_{2xm}(x-w_1)] \\
 & + B_{2m} \cos[k_{2xm}(x-w_1)] \} - \\
 & \frac{k_z}{\omega\mu_0} \sum_{m=1}^{M_2} \frac{d\tilde{\psi}_{2m}(y)}{dy} \{ -\tilde{A}_{2m} \tilde{k}_{2xm} \cos[\tilde{k}_{2xm}(x-w_1)] \\
 & + \tilde{B}_{2m} \sin[\tilde{k}_{2xm}(x-w_1)] \}
 \end{aligned}$$

The equations for region 3 are identical to those for region 2 with subscript "2" substituted by subscript "3".

#### REGION 4

Electric field components:

$$\begin{aligned}
 E_{4x} = & \frac{1}{j\omega\epsilon_4(y)} \sum_{m=1}^{M_4} \frac{d\psi_{4m}(y)}{dy} jk_{4xm} \exp[-jk_{4xm}(x-w_2)] A_{4m} - \\
 & jk_z \sum_{m=1}^{M_4} \tilde{\psi}_{4m}(y) \exp[-j\tilde{k}_{4xm}(x-w_2)] \tilde{A}_{4m}
 \end{aligned}$$

$$E_{4y} = \frac{1}{j\omega\epsilon_4(y)} \sum_{m=1}^{M_4} (k_z^2 + k_{4xm}^2) \psi_{4m}(y) \exp[-jk_{4xm}(x-w_2)] A_{4m} \quad (3.1.11.a)$$

$$E_{4z} = -\frac{k_z}{\omega\epsilon_4(y)} \sum_{m=1}^{M_4} \frac{d\psi_{4m}(y)}{dy} \exp[-jk_{4xm}(x-w_2)] A_{4m} +$$

$$\sum_{m=1}^{M_4} \tilde{\psi}_{4m}(y) j\tilde{k}_{4xm} \exp[-j\tilde{k}_{4xm}(x-w_2)] \tilde{A}_{4m}$$

Magnetic field components:

$$H_{4x} = jk_z \sum_{m=1}^{M_1} \psi_{4m}(y) \exp[k_{4xm}(x-w_2)] A_{4m} -$$

$$\frac{1}{j\omega\mu_0} \sum_{m=1}^{M_4} \frac{d\tilde{\psi}_{4m}(y)}{dy} j\tilde{k}_{4xm} \exp[-j\tilde{k}_{4xm}(x-w_2)] \tilde{A}_{4m}$$

$$H_{4y} = \frac{1}{j\omega\mu_0} \sum_{m=1}^{M_4} (k_z^2 + \tilde{k}_{4xm}^2) \tilde{\psi}_{4m}(y) \exp[-j\tilde{k}_{4xm}(x-w_2)] \tilde{A}_{4m} \quad (3.1.11.b)$$

$$H_{4z} = \sum_{m=1}^{M_4} \psi_{4m}(y) jk_{4xm} \exp[-jk_{4xm}(x-w_2)] A_{4m} -$$

$$\frac{k_z}{\omega\mu_0} \sum_{m=1}^{M_4} \frac{d\tilde{\psi}_{4m}(y)}{dy} \exp[-j\tilde{k}_{4xm}(x-w_2)] \tilde{A}_{4m}$$

In the above equations, the sums have been truncated at  $M_1$  modes for the fields in region 1,  $M_2$  modes for those in region 2, etc. For the solution of this system of equations to be

unique, these equations must form a square matrix, which means that :

$$2M_2 + 2M_3 = M_1 + M_4 \quad (3.1.12)$$

The relationship in eq. (3.1.12) ensures that the system of equations will have a unique solution. It does not, however, ensure convergence of the system. This is because one very important geometrical factor has not been considered yet. All planar structures have discontinuities in the form of sharp edges. It was noted earlier in this chapter that these discontinuities must conform to the edge condition, that is, the power of the electric and magnetic fields at these points must be finite. This condition was found to be adequately met when the number of modes retained in each region were such that:

$$\frac{M_1}{M_3} = \frac{M_4}{M_3} = \frac{h}{h-h_3} \quad (3.1.13)$$

and

$$\frac{M_1}{M_3} = \frac{M_4}{M_3} = \frac{h}{h-h_3} \quad (3.1.14)$$

Thus, the edge condition will yield a relationship between the number of modes which should be retained in each region, and their relative dimensions.

Matching the tangential fields at the interface  $x=w_1$  and  $0 \leq y \leq h_3$  yields:

$$\begin{aligned}
E_{1y}(x=w_1) &= E_{2y}(x=w_1) \Leftrightarrow \\
\frac{1}{j\omega\epsilon_1(y)} \sum_{m=1}^{M_1} (k_z^2 + k_{1xm}^2) \psi_{1m}(y) \frac{\cos(k_{1xm}w_1)}{\sin f} A_{1m} & \quad (3.1.15.a) \\
= \frac{1}{j\omega\epsilon_2(y)} \sum_{m=1}^{M_2} (k_z^2 + k_{1xm}^2) \psi_{1m}(y) A_{2m}
\end{aligned}$$

$$\begin{aligned}
E_{1z}(x=w_1) &= E_{2z}(x=w_1) \Leftrightarrow \\
-\frac{k_z}{\omega\epsilon_1(y)} \sum_{m=1}^{M_1} \frac{d\psi_{1m}(y)}{dy} \frac{\cos(k_{1xm}w_1)}{\sin f} A_{1m} & \quad (3.1.15.b) \\
- \sum_{m=1}^{M_1} \tilde{\psi}_{1m}(y) \begin{pmatrix} 1 \\ -\tilde{k}_{1xm} \end{pmatrix} \frac{\cos(\tilde{k}_{1xm}w_1)}{\sin} \tilde{A}_{1m} = \\
- \frac{k_z}{\omega\epsilon_2(y)} \sum_{m=1}^{M_2} \frac{d\psi_{2m}(y)}{dy} A_{2m} - \sum_{\mu=1}^{M_2} \tilde{\psi}_{2m}(y) \tilde{B}_{2m}
\end{aligned}$$

$$\begin{aligned}
H_{1y}(x=w_1) &= H_{2y}(x=w_1) \Leftrightarrow \\
\frac{1}{j\omega\mu_0} \sum_{m=1}^{M_1} (k_z^2 + \tilde{k}_{1xm}^2) \tilde{\psi}_{1m}(y) \frac{\sin f}{\cos} (\tilde{k}_{1xm}w_1) \tilde{A}_{1m} & \quad (3.1.15.c) \\
= \frac{1}{j\omega\mu_0} \sum_{m=1}^{M_2} (k_z^2 + \tilde{k}_{2xm}^2) \tilde{\psi}_{2m}(y) \tilde{A}_{2m}
\end{aligned}$$



$$\begin{aligned}
H_{1z}(x=w_1) &= H_{2z}(x=w_1) \Leftrightarrow \\
\sum_{m=1}^{M_1} \psi_{1m}(y) \begin{pmatrix} -k_{1xm} \\ 1 \end{pmatrix} \frac{\sin(k_{1xm}w_1)}{\cos(k_{1xm}w_1)} A_{1m} & \\
-\frac{k_z}{\omega\mu_0} \sum_{m=1}^{M_1} \frac{d\tilde{\psi}_{1m}(y)}{dy} \frac{\sin(\tilde{k}_{1xm}w_1)}{\cos(\tilde{k}_{1xm}w_1)} \tilde{A}_{1m} &= \\
\sum_{m=1}^{M_2} \psi_{2m}(y) B_{2m} - \frac{k_z}{\omega\mu_0} \sum_{\mu=1}^{M_2} \frac{d\tilde{\psi}_{2\mu}(y)}{dy} \tilde{A}_{2\mu} &
\end{aligned} \tag{3.1.15.d}$$

Matching tangential electric and magnetic fields at  $x=w_2$  for  $0 \leq y \leq h_3$  yields:

$$\begin{aligned}
 E_{2y}(x=w_2) &= E_{4y}(x=w_2) \Leftrightarrow \\
 \frac{1}{j\omega\epsilon_2(y)} \sum_{m=1}^{M_2} (k_z^2 + k_{2xm}^2) \psi_{2m}(y) \{ &A_{2m} \cos[k_{2xm}(w_2 - w_1)] \\
 + B_{2m} \sin[k_{2xm}(w_2 - w_1)] \} &= \\
 \frac{1}{j\omega\epsilon_4(y)} \sum_{m=1}^{M_4} (k_z^2 + k_{4xm}^2) \psi_{4m}(y) A_{4m} &
 \end{aligned} \tag{3.1.16.a}$$

$$\begin{aligned}
 E_{2z}(x=w_2) &= E_{4z}(x=w_2) \Leftrightarrow \\
 -\frac{k_z}{\omega\epsilon_2(y)} \sum_{m=1}^{M_2} \frac{d\psi_{2m}(y)}{dy} \{ &A_{2m} \cos[k_{2xm}(w_2 - w_1)] \\
 + B_{2m} \sin[k_{2xm}(w_2 - w_1)] \} &- \\
 \sum_{m=1}^{M_1} \tilde{\psi}_{2m}(y) \{ -\tilde{A}_{2m} \tilde{k}_{2xm} \sin[\tilde{k}_{2xm}(w_2 - w_1)] & \\
 + \tilde{B}_{2m} \cos[\tilde{k}_{2xm}(w_2 - w_1)] \} &= \\
 -\frac{k_z}{\omega\epsilon_4(y)} \sum_{m=1}^{M_4} \frac{d\psi_{4m}(y)}{dy} A_{4m} + \sum_{\mu=1}^{M_4} \tilde{\psi}_{4m}(y) j\tilde{k}_{4xm} \tilde{A}_{4m} &
 \end{aligned} \tag{3.1.16.b}$$

$$\begin{aligned}
 H_{2y}(x=w_2) &= H_{4y}(x=w_2) \Leftrightarrow \\
 \frac{1}{j\omega\mu_0} \sum_{m=1}^{M_2} (k_z^2 + \tilde{k}_{2xm}^2) \tilde{\psi}_{2m}(y) \{ &\tilde{A}_{2m} \cos[\tilde{k}_{2xm}(w_2 - w_1)] \\
 + \tilde{B}_{2m} \sin[\tilde{k}_{2xm}(w_2 - w_1)] \} &= \\
 \frac{1}{j\omega\mu_0} \sum_{m=1}^{M_4} (k_z^2 + \tilde{k}_{4xm}^2) \tilde{\psi}_{4m}(y) \tilde{A}_{4m} &
 \end{aligned} \tag{3.1.16.c}$$

$$\begin{aligned}
H_{2z}(x=w_2) &= H_{4z}(x=w_2) \Leftrightarrow \\
\sum_{m=1}^{M_2} \psi_{2m}(y) \{ &-A_{2m}k_{2xm}\sin[k_{2xm}(w_2-w_1)] \\
&+B_{2m}\cos[k_{2xm}(w_2-w_1)] \} - \\
-\frac{k_z}{\omega\mu_0} \sum_{m=1}^{M_1} \frac{d\tilde{\psi}_{2m}(y)}{dy} \{ &\tilde{A}_{2m}\cos[\tilde{k}_{2xm}(w_2-w_1)] \\
&+\tilde{B}_{2m}\sin[\tilde{k}_{2xm}(w_2-w_1)] \} = \\
-\sum_{m=1}^{M_4} \psi_{4m}(y)jk_{4xm}A_{4m} &+\frac{k_z}{\omega\mu_0} \sum_{\mu=1}^{M_4} \frac{d\tilde{\psi}_{4\mu}(y)}{dy} \tilde{A}_{4\mu}
\end{aligned} \tag{3.1.16.d}$$

The equations for  $x=w_1$  and  $x=w_2$  with  $h_3 \leq y \leq h$  are identical to the corresponding equations for  $0 \leq y \leq h_3$  with the subscript "3" substituted for subscript "2".

As stated earlier, the orthogonality of the modal expansion functions  $\psi_{im}(y)$  and  $\tilde{\psi}_{im}(y)$  take the form:

$$\int_{\text{over one region}} \frac{1}{\epsilon_i(y)} \psi_{im}(y) \psi_{in}(y) dy \quad \text{for } m \neq n \tag{3.1.17}$$

and:

$$\int_{\text{over one region}} \tilde{\psi}_{im}(y) \tilde{\psi}_{in}(y) dy \quad \text{for } m \neq n \tag{3.1.18}$$

So, orthogonality can be utilized here to reduce the complexity of the continuity equations. By multiplying each equation by the appropriate orthogonal function, and integrating over the appropriate region (from 0 to  $h_3$ ), the equations for  $0 \leq y \leq h_3$  may be rewritten as:

$$\begin{aligned}
& \sum_{m=1}^{M_1} (k_z^2 + k_{1xm}^2) I_{1mn}^2 \frac{\cos}{\sin f} (k_{1xm} w_1) A_{1m} \\
& = (k_z^2 + k_{1xn}^2) I_{2nn}^2 A_{2n}
\end{aligned} \tag{3.1.18.a}$$

$$\begin{aligned}
& \frac{k_z}{\omega} \sum_{m=1}^{M_1} I_{1mn}^2 \frac{\cos}{\sin f} (k_{1xm} w_1) A_{1m} \\
& + \sum_{m=1}^{M_1} I_{2mn}^2 \left( \begin{array}{c} 1 \\ -\tilde{k}_{1xm} \end{array} \right) \frac{\cos}{\sin} (\tilde{k}_{1xm} w_1) \tilde{A}_{1m} \\
& = \frac{k_z}{\omega} \sum_{m=1}^{M_2} I_{3mn}^2 A_{2m} - I_{4nn}^2 \tilde{B}_{2n}
\end{aligned} \tag{3.1.18.b}$$

$$\begin{aligned}
& \sum_{m=1}^{M_1} (k_z^2 + \tilde{k}_{1xm}^2) I_{2mn}^2 \frac{\sin f}{\cos} (\tilde{k}_{1xm} w_1) \tilde{A}_{1m} \\
& = (k_z^2 + \tilde{k}_{2xn}^2) I_{4nn}^2 \tilde{A}_{2n}
\end{aligned} \tag{3.1.18.c}$$

$$\begin{aligned}
& \sum_{m=1}^{M_1} I_{1mn}^2 \left( \begin{array}{c} -k_{1xm} \\ 1 \end{array} \right) \frac{\sin}{\cos} (k_{1xm} w_1) A_{1m} \\
& - \frac{k_z}{\omega \mu_0} \sum_{m=1}^{M_1} I_{3mn}^2 \frac{\sin d}{\cos} (\tilde{k}_{1xm} w_1) \tilde{A}_{1m} \\
& = I_{2nn}^2 B_{2m} - \frac{k_z}{\omega \mu_0} \sum_{\mu=1}^{M_2} I_{4mn}^2 \tilde{A}_{2m}
\end{aligned} \tag{3.1.18.d}$$

$$\begin{aligned}
& (k_z^2 + k_{2xn}^2) I_{2nn}^{e2} \{ A_{2n} \cos[k_{2xn}(w_2 - w_1)] \\
& + B_{2n} \sin[k_{2xn}(w_2 - w_1)] \} = \quad (3.1.18.e) \\
& \sum_{m=1}^{M_4} (k_z^2 + k_{4xm}^2) I_{1mn}^{e2} A_{4m}
\end{aligned}$$

$$\begin{aligned}
& - \frac{k_z}{\omega} \sum_{m=1}^{M_2} I_{3mn}^{h2} \{ A_{2m} \cos[k_{2xm}(w_2 - w_1)] + B_{2m} \sin[k_{2xm}(w_2 - w_1)] \} - \\
& I_{4nn}^{h2} \{ -\tilde{A}_{2n} \tilde{k}_{2xn} \sin[\tilde{k}_{2xn}(w_2 - w_1)] + \tilde{B}_{2n} \cos[\tilde{k}_{2xn}(w_2 - w_1)] \} = \quad (3.1.18.f) \\
& - \frac{k_z}{\omega} \sum_{m=1}^{M_4} I_{1mn}^{h2} A_{4m} + \sum_{m=1}^{M_4} I_{2mn}^{h2} \tilde{k}_{4xm} \tilde{A}_{4m}
\end{aligned}$$

$$\begin{aligned}
& (k_z^2 + \tilde{k}_{2xn}^2) I_{4nn}^{h2} \{ \tilde{A}_{2n} \cos[\tilde{k}_{2xn}(w_2 - w_1)] + \tilde{B}_{2n} \sin[\tilde{k}_{2xn}(w_2 - w_1)] \} = \quad (3.1.18.g) \\
& \sum_{m=1}^{M_4} (k_z^2 + \tilde{k}_{4xm}^2) I_{2mn}^{h2} \tilde{A}_{4m}
\end{aligned}$$

$$\begin{aligned}
& I_{2nn}^{e2} \{ -A_{2n} k_{2xn} \sin[k_{2xn}(w_2 - w_1)] + B_{2n} \cos[k_{2xn}(w_2 - w_1)] \} \\
& - \frac{k_z}{\omega \mu_0} \sum_{m=1}^{M_1} I_{4mn}^{e2} \{ \tilde{A}_{2m} \cos[\tilde{k}_{2xm}(w_2 - w_1)] + \tilde{B}_{2m} \sin[\tilde{k}_{2xm}(w_2 - w_1)] \} = \quad (3.1.18.h) \\
& - \sum_{m=1}^{M_4} I_{1mn}^{e2} \tilde{k}_{4xm} A_{4m} + \frac{k_z}{\omega \mu_0} \sum_{\mu=1}^{M_4} I_{3mn}^{e2} \tilde{A}_{4m}
\end{aligned}$$

where:

$$I_{1mn}^{ei} = \int_0^{h_3} \frac{1}{\varepsilon(y)} \psi_{1m}(y) \psi_{in}(y) dy = \int_0^{h_3} \psi_{4m}(y) \psi_{in}(y) dy$$

$$I_{2mn}^{ei} = \int_0^{h_3} \frac{1}{\varepsilon(y)} \psi_{im}(y) \psi_{in}(y) dy$$

$$I_{3mn}^{ei} = \int_0^{h_3} \frac{1}{\varepsilon(y)} \frac{d\tilde{\psi}_{1m}(y)}{dy} \psi_{in}(y) dy = \int_0^{h_3} \frac{1}{\varepsilon(y)} \frac{d\tilde{\psi}_{4m}(y)}{dy} \psi_{in}(y) dy$$

$$I_{4mn}^{ei} = \int_0^{h_3} \frac{1}{\varepsilon(y)} \frac{d\tilde{\psi}_{im}(y)}{dy} \psi_{in}(y) dy$$

$$I_{5mn}^e = \int_0^h \frac{1}{\varepsilon(y)} \psi_{1m}(y) \psi_{1n}(y) dy = \int_0^h \frac{1}{\varepsilon(y)} \psi_{4m}(y) \psi_{4n}(y) dy$$

$$I_{6mn}^e = \int_0^h \frac{1}{\varepsilon(y)} \frac{d\tilde{\psi}_{1m}(y)}{dy} \psi_{1n}(y) dy = \int_0^h \frac{1}{\varepsilon(y)} \frac{d\tilde{\psi}_{4m}(y)}{dy} \psi_{4n}(y) dy$$

$$I_{1mn}^{hi} = \int_0^{h_3} \frac{1}{\varepsilon(y)} \frac{d\psi_{1m}(y)}{dy} \tilde{\psi}_{in}(y) dy = \int_0^{h_3} \frac{1}{\varepsilon(y)} \frac{d\psi_{4m}(y)}{dy} \tilde{\psi}_{in}(y) dy$$

$$I_{2mn}^{hi} = \int_0^{h_3} \tilde{\psi}_{1m}(y) \tilde{\psi}_{in}(y) dy = \int_0^{h_3} \tilde{\psi}_{4m}(y) \tilde{\psi}_{in}(y) dy$$

$$I_{3mn}^{hi} = \int_0^{h_3} \frac{1}{\varepsilon(y)} \frac{d\psi_{im}(y)}{dy} \tilde{\psi}_{in}(y) dy$$

$$I_{4mn}^h = \int_0^{h_3} \tilde{\psi}_{im}(y) \psi_{in}(y) dy$$

$$I_{5mn}^h = \int_0^h \tilde{\psi}_{1m}(y) \tilde{\psi}_{1n}(y) dy = \int_0^h \tilde{\psi}_{4m}(y) \tilde{\psi}_{4n}(y) dy$$

$$I_{6mn}^h = \int_0^h \frac{1}{\varepsilon(y)} \frac{d\psi_{1m}(y)}{dy} \tilde{\psi}_{1n}(y) dy = \int_0^h \frac{1}{\varepsilon(y)} \frac{d\psi_{4m}(y)}{dy} \tilde{\psi}_{4n}(y) dy$$

where  $i=2,3$ , for regions 2 and 3, correspondingly. Thus, an identical set of equations as those derived for  $h \leq y \leq h_3$  may be derived for the case  $h_3 \leq y \leq h$ . For this case, it is sufficient to substitute  $i=3$  instead of 2 in the superscript in the orthogonalization integrals, and substitute 3 for 2 in the subscript of the remaining functions.

By developing the above equations further, the final form of the set of eigenvalue equations is derived for  $0 \leq y \leq h_3$ :

$$\begin{aligned} & \frac{k_z}{\omega} \sum_{m=1}^{M_1} \left\{ I_{1mn}^{h2} \cos(k_{1xm} w_1) - (k_z^2 + k_{1xm}^2) \left[ \sum_{p=1}^{M_1} \frac{I_{3pn}^{h2} I_{1mp}^{e2}}{(k_z^2 + k_{2xp}^2) I_{2pp}^{e2}} \right] \cos(k_{1xm} w_1) \right\} A_{1m} + \\ & \sum_{m=1}^{M_1} I_{2mn}^{h2} \left\{ \begin{pmatrix} 1 \\ -\tilde{k}_{1xm} \end{pmatrix} \cos(\tilde{k}_{1xm} w_1) + \frac{(k_z^2 + \tilde{k}_{1xm}^2)}{(k_z^2 + k_{2xn}^2)} \frac{\sin(\tilde{k}_{1xm} w_1) \tilde{k}_{2xn} \cot[\tilde{k}_{2xn}(w_2 - w_1)]}{\cos(\tilde{k}_{1xm} w_1)} \right\} \tilde{A}_{1m} - \\ & \sum_{m=1}^{M_4} \frac{(k_z^2 + k_{4xm}^2)}{(k_z^2 + k_{2xn}^2)} I_{2mn}^{h2} \frac{1}{\sin[\tilde{k}_{2xn}(w_2 - w_1)]} \tilde{A}_{4m} = 0 \end{aligned} \quad (3.1.19.a)$$

$$\begin{aligned} & \sum_{m=1}^{M_1} I_{1mn}^{e2} \left\{ \begin{pmatrix} -k_{1xm} \\ 1 \end{pmatrix} \frac{\sin(k_{1xm} w_1)}{\cos(k_{1xm} w_1)} + \frac{(k_z^2 + k_{1xm}^2)}{(k_z^2 + k_{2xn}^2)} \frac{\cos(k_{1xm} w_1) \cos[k_{2xn}(w_2 - w_1)]}{\sin[k_{2xn}(w_2 - w_1)]} \right\} A_{1m} - \\ & \frac{k_z}{\omega \mu_0} \sum_{m=1}^{M_1} \left\{ I_{3mn}^{e2} \sin(\tilde{k}_{1xm} w_1) - (k_z^2 + \tilde{k}_{1xm}^2) \left[ \sum_{p=1}^{M_1} \frac{I_{4pn}^{e2} I_{2mp}^{h2}}{(k_z^2 + k_{2xp}^2) I_{4pp}^{h2}} \right] \sin(\tilde{k}_{1xm} w_1) \right\} \tilde{A}_{1m} - \\ & \sum_{m=1}^{M_4} \frac{(k_z^2 + k_{4xm}^2)}{(k_z^2 + k_{2xn}^2)} I_{1mn}^{e2} \frac{1}{\sin[\tilde{k}_{2xn}(w_2 - w_1)]} A_{4m} = 0 \end{aligned} \quad (3.1.19.b)$$

$$\begin{aligned}
& - \sum_{m=1}^{M_1} \frac{(k_z^2 + k_{1xm}^2)}{(k_z^2 + k_{2xn}^2)} I_{1mn}^{e2} \cos(k_{1xm} w_1) A_{1m} + \\
& \sum_{m=1}^{M_1} I_{1mn}^{e2} \left\{ \frac{(k_z^2 + k_{4xm}^2)}{(k_z^2 + k_{2xn}^2)} \cos[k_{2xn}(w_2 - w_1)] + j k_{4xm} \sin[k_{2xn}(w_2 - w_1)] \right\} A_{4m} - \\
& \frac{k_z}{\omega \mu_0} \sum_{m=1}^{M_4} \left\{ (k_z^2 + \tilde{k}_{4xm}^2) \sum_{p=1}^{M_2} \frac{I_{4pn}^{e2} I_{2mp}^{h2}}{(k_z^2 + \tilde{k}_{2xp}^2) I_{4pp}^{h2}} - I_{3mn}^{e2} \right\} \sin[k_{2xn}(w_2 - w_1)] \tilde{A}_{4m} = 0
\end{aligned}
\tag{3.1.19.c}$$

$$\begin{aligned}
& \sum_{m=1}^{M_1} \frac{(k_z^2 + \tilde{k}_{1xm}^2)}{(k_z^2 + \tilde{k}_{2xn}^2)} I_{2mn}^{h2} \sin(\tilde{k}_{1xm} w_1) \tilde{A}_{1m} - \\
& \frac{k_z}{\omega} \sum_{m=1}^{M_4} \left\{ (k_z^2 + k_{4xm}^2) \left[ \sum_{p=1}^{M_2} \frac{I_{3pn}^{h2} I_{1mp}^{e2}}{(k_z^2 + k_{2xp}^2) I_{2pp}^{e2}} \right] \sin[k_{2xn}(w_2 - w_1)] - I_{1mn}^{h2} \sin[k_{2xn}(w_2 - w_1)] \right\} A_{4m} - \\
& \sum_{m=1}^{M_4} I_{2mn}^{h2} \left\{ \frac{(k_z^2 + \tilde{k}_{4xm}^2)}{(k_z^2 + \tilde{k}_{2xn}^2)} \cos[\tilde{k}_{2xn}(w_2 - w_1)] + j \tilde{k}_{4xm} \sin[\tilde{k}_{2xn}(w_2 - w_1)] \right\} \tilde{A}_{4m} = 0
\end{aligned}
\tag{3.1.19.d}$$

As before, substituting the corresponding variables for region 3 will yield the corresponding equations for  $h_3 \leq y \leq h$ .

The above set of equations may be expressed as a homogeneous matrix equation  $[A]x=0$ , where  $[A]$  is the matrix of the coefficients of  $A_{1m}$ ,  $\tilde{A}_{1m}$ ,  $A_{4m}$ , and  $\tilde{A}_{4m}$   $x$  is the vector containing  $A_{1m}$ ,  $\tilde{A}_{1m}$ ,  $A_{4m}$ , and  $\tilde{A}_{4m}$ . This homogeneous equation has a nontrivial solution only for the case  $\det(A)=0$ . The coefficients of the matrix  $[A]$  have only one unknown variable,  $k_z$ , so solving the equation  $\det(A)=0$  yields the solution for the



propagation constant. By substituting this value of  $k_z$  back into the set of equations  $[A]x=0$ , an underdetermined system is derived for determining the coefficients  $A_{1m}$ ,  $\tilde{A}_{1m}$ ,  $A_{1m}$ , and  $\tilde{A}_{4m}$  of the electric and magnetic fields of the structure.

After solving for the coefficients of the fields in regions 1 and 4, the remaining electric and magnetic field coefficients are determined by:

$$A_{im} = \sum_{p=1}^{M_1} \frac{(k^2 - k_{1yp}^2)}{(k^2 - k_{iym}^2)} \frac{I_{1pm}^{ei}}{I_{2mm}^{ei}} \cos(k_{1xp} w_1) A_{1p} \quad (3.1.20.a)$$

$$B_{im} = \sum_{p=1}^{M_1} \frac{I_{3pm}^{ei}}{I_{2mm}^{ei}} \begin{pmatrix} -k_{ixp} \\ 1 \end{pmatrix} \frac{\sin(k_{1xp} w_1)}{\cos(k_{1xp} w_1)} A_{1p}$$

$$\frac{k_z}{\omega \mu_0} \sum_{p=1}^{M_1} \frac{I_{4pm}^{ei}}{I_{2mm}^{ei}} \frac{\sin(\tilde{k}_{1xp} w_1)}{\cos(\tilde{k}_{1xp} w_1)} \tilde{A}_{1p}$$

$$\frac{k_z}{\omega \mu_0} \sum_{p=1}^{M_1} (k^2 - \tilde{k}_{1yp}^2) \frac{\sin(\tilde{k}_{1xp} w_1)}{\cos(\tilde{k}_{1xp} w_1)} \left\{ \sum_{l=1}^{M_1} \frac{I_{5lm}^{ei} I_{2pl}^{hi}}{I_{41l}^{hi} (k^2 - \tilde{k}_{ilyl}^2)} \right\} \tilde{A}_{1p} \quad (3.1.20.b)$$

$$\tilde{A}_{im} = \sum_{p=1}^{M_1} \frac{(k^2 - \tilde{k}_{1yp}^2)}{(k^2 - \tilde{k}_{iym}^2)} \frac{I_{2pm}^{hi}}{I_{4mm}^{hi}} \frac{\sin(\tilde{k}_{1xp} w_1)}{\cos(\tilde{k}_{1xp} w_1)} \tilde{A}_{1p} \quad (3.1.20.c)$$

$$\begin{aligned}
\tilde{B}_{im} &= \frac{k_z}{\omega} \sum_{p=1}^{M_1} \frac{I_{1pm}^{hi}}{I_{4mm}^{hi}} \frac{\cos(k_{1xp} w_1)}{\sin(k_{1xp} w_1)} A_{1p}^- \\
\frac{k_z}{\omega} \sum_{p=1}^{M_1} (k^2 - k_{1yp}^2) \frac{\cos(k_{1xp} w_1)}{\sin(k_{1xp} w_1)} &\left\{ \sum_{l=1}^{M_i} \frac{I_{3lm}^{hi} I_{1pl}^{ei}}{I_{21l}^{ei} (k^2 - k_{ily}^2)} \right\} A_{1p}^+ \\
\sum_{p=1}^{M_1} I_{2pm}^{hi} \begin{pmatrix} 1 \\ -\tilde{k}_{1xp} \end{pmatrix} \frac{\cos(\tilde{k}_{1xp} w_1)}{\sin(\tilde{k}_{1xp} w_1)} &\tilde{A}_{1p}
\end{aligned}
\tag{3.1.20.d}$$

The coefficients determined through the matrix equation are determined within a multiplicative constant, so in fact the electric and magnetic field distribution in each region, if not their true amplitude, may be derived.

### 3.2. Characteristic Impedance

Theoretically, three different expressions may be used to calculate the characteristic impedance of any device. When applied to the coupled microstrip line, these three expressions define the relationship between the characteristic impedance of the coupled microstrip line, the time-averaged power flow in the strip, the complex voltage of the strip calculated at the center of the strip, and the current of the strip.

The power-voltage relationship gives the characteristic impedance of the coupled microstrip line as a function of the time-averaged power flow in the strip,  $P_{avg}$ , and the complex voltage  $V$  of the strip, calculated at the center of the strip. In the case of the coupled microstrip line, the characteristic impedance would then be:

$$Z_0 = \frac{VV^*}{P_{avg}} \quad (3.2.1)$$

The power-current relationship gives the characteristic impedance of the coupled microstrip line as a function of  $P_{avg}$ , and the complex current  $I$  on the strip, and is given by:

$$Z_0 = \frac{P_{avg}}{II^*} \quad (3.2.2)$$

The voltage-current relationship gives the characteristic impedance of the coupled microstrip line as a function of the complex voltage,  $V$ , and the complex current,  $I$ , of the strip, and is given by:

$$Z_0 = \frac{V}{I} \quad (3.2.3)$$

Although experiments have shown the power-current calculation to be more valid in the case of the microstrip line, all three calculations will be presented in this work.

The power,  $P_{avg}$  is calculated using the Poynting vector, which is defined as:

$$P = \frac{1}{2} \text{Re} \iint_s \{ \mathbf{E} \times \mathbf{H}^* \cdot \mathbf{a}_z \} dx dy$$

Using the rectangular components of the electric and magnetic fields, the Poynting vector may be written as:

$$P = \frac{1}{2} \text{Re} \iint_s \{ E_x H_y^* - E_y H_x^* \} dx dy$$

Using the relationships in (3.1.8) through (3.1.11) to express the fields in terms of the scalar potential functions in each region, a Poynting vector may be calculated for each region of the coupled microstrip line.

The power in region 1 is thus calculated as:

$$\begin{aligned}
P_1 &= \frac{1}{2} \operatorname{Re} \int_0^h dy \int_0^{w_1} dx (E_{1y} H_{1x}^* - E_{1x} H_{1y}^*) \\
&= \frac{1}{\omega^2 \mu_0} \sum_{m=1}^{M_1} \sum_{n=1}^{M_1} (k^2 - \tilde{k}_{1yn}^2) I_{6mn}^h \begin{pmatrix} -k_{1xm} \\ 1 \end{pmatrix} \frac{I_2}{I_1} (0, w_1, k_{1xm}, 0, \tilde{k}_{1xn}, 0) A_{1m} \tilde{A}_{1n} + \\
&\quad \frac{k_z}{\omega \mu_0} \sum_{m=1}^{M_1} (k^2 - \tilde{k}_{1ym}^2) I_{5mm}^h \frac{I_2}{I_1} (0, w_1, \tilde{k}_{1xm}, 0, \tilde{k}_{1xm}, 0) \tilde{A}_{1m}^2 + \\
&\quad \frac{k_z}{\omega} \sum_{m=1}^{M_1} (k^2 - k_{1ym}^2) I_{5mm}^e \frac{I_1}{I_2} (0, w_1, k_{1xm}, 0, k_{1xm}, 0) A_{1m}^2 + \\
&\quad \frac{1}{\omega^2 \mu_0} \sum_{m=1}^{M_1} \sum_{n=1}^{M_1} (k^2 - k_{1yn}^2) I_{6nm}^e \begin{pmatrix} 1 \\ -k_{1xn}^2 \end{pmatrix} \frac{I_1}{I_2} (0, w_1, k_{1xm}, 0, \tilde{k}_{1xn}, 0) A_{1m} \tilde{A}_{1n} +
\end{aligned}$$

where the functions  $I_1$ - $I_3$  are defined as:

$$I_1(l, ul, a, b, c, d) = \int_{l_1}^{ul} \cos[a \cdot (x-b)] \cdot \cos[c \cdot (x-d)] \cdot dx$$

$$I_2(l, ul, a, b, c, d) = \int_{l_1}^{ul} \sin[a \cdot (x-b)] \cdot \sin[c \cdot (x-d)] \cdot dx$$

$$I_3(l, ul, a, b, c, d) = \int_{l_1}^{ul} \cos[a \cdot (x-b)] \cdot \sin[c \cdot (x-d)] \cdot dx$$

and the other parameters have been defined in section 3.1.

The power in regions 2 and 3 are calculated as:

$$\begin{aligned}
P_i &= \frac{1}{2} \operatorname{Re} \int_0^h dy \int_{w_1}^{w_2} dx (E_{ix} H_{iy}^* - E_{iy} H_{ix}^*) \\
&= \frac{1}{\omega^2 \mu_0} \sum_{m=1}^{M_i} \sum_{n=1}^{M_i} (k^2 - \tilde{k}_{iyn}^2) I_{3mn}^{hi} \mathcal{LNT}1_{mn}^i - \\
&\quad \frac{k_z}{\omega \mu_0} \sum_{m=1}^{M_i} (k^2 - \tilde{k}_{iyn}^2) I_{4mm}^{hi} \mathcal{LNT}2_{mm}^i + \\
&\quad \frac{k_z}{\omega} \sum_{m=1}^{M_i} (k^2 - k_{iym}^2) I_{2mm}^{ei} \mathcal{LNT}3_{mm}^i + \\
&\quad \frac{1}{\omega} \sum_{m=1}^{M_i} \sum_{n=1}^{M_i} (k^2 - k_{iym}^2) I_{4nm}^{ei} \mathcal{LNT}4_{mn}^i
\end{aligned}$$

where  $i=2$  or  $3$ , for region 2 or 3, correspondingly. The functions  $\mathcal{LNT}1$  through  $\mathcal{LNT}4$  are defined as:

$$\begin{aligned}
\mathcal{LNT}1_{mn}^i &= -A_{im} k_{ixm}^2 \tilde{A}_{in} I_3(w_1, w_2, \tilde{k}_{ixn}, w_1, k_{ixm}, w_1) + \\
&\quad B_{im} A_{in} I_1(w_1, w_2, k_{ixm}, w_1, \tilde{k}_{ixn}, w_1) - \\
&\quad A_{im} k_{ixm}^2 \tilde{B}_{in} I_2(w_1, w_2, k_{ixm}, w_1, \tilde{k}_{ixn}, w_1) + \\
&\quad B_{im} \tilde{B}_{in} I_3(w_1, w_2, k_{ixm}, w_1, \tilde{k}_{ixn}, w_1) \\
\mathcal{LNT}2_{mn}^i &= \tilde{A}_{im} \tilde{A}_{in} I_1(w_1, w_2, \tilde{k}_{ixm}, w_1, \tilde{k}_{ixn}, w_1) + \\
&\quad \tilde{A}_{im} \tilde{B}_{in} I_3(w_1, w_2, \tilde{k}_{ixm}, w_1, \tilde{k}_{ixn}, w_1) + \\
&\quad \tilde{B}_{im} \tilde{A}_{in} I_3(w_1, w_2, \tilde{k}_{ixn}, w_1, \tilde{k}_{ixm}, w_1) + \\
&\quad \tilde{B}_{im} \tilde{B}_{in} I_2(w_1, w_2, \tilde{k}_{ixm}, w_1, \tilde{k}_{ixn}, w_1)
\end{aligned}$$

$$\begin{aligned} \text{INT}3_{mn}^i &= A_{im}A_{in}I_1(w_1, w_2, k_{ixm}, w_1, k_{ixn}, w_1) + \\ &B_{im}A_{in}I_3(w_1, w_2, k_{ixn}, w_1, k_{ixm}, w_1) + \\ &A_{im}B_{in}I_3(w_1, w_2, k_{ixm}, w_1, k_{ixn}, w_1) + \\ &B_{im}B_{in}I_2(w_1, w_2, k_{ixm}, w_1, k_{ixn}, w_1) \end{aligned}$$

$$\begin{aligned} \text{INT}4_{mn}^i &= -A_{im}\tilde{A}_{in}\tilde{k}_{ixn}^2 I_3(w_1, w_2, k_{ixm}, w_1, \tilde{k}_{ixn}, w_1) + \\ &A_{im}\tilde{B}_{in}I_1(w_1, w_2, k_{ixm}, w_1, \tilde{k}_{ixn}, w_1) - \\ &B_{im}\tilde{A}_{in}\tilde{k}_{ixn}^2 I_2(w_1, w_2, k_{ixm}, w_1, \tilde{k}_{ixn}, w_1) + \\ &B_{im}\tilde{B}_{in}I_3(w_1, w_2, \tilde{k}_{ixn}, w_1, k_{ixm}, w_1) \end{aligned}$$

The power in region 4 is:

$$\begin{aligned} P_4 &= \frac{1}{2} \text{Re} \int_0^h dy \int_{w_2}^\infty dx (E_{4x} \cdot H_{4y}^* - E_{4y} \cdot H_{4x}^*) \\ &= \frac{1}{\omega^2 \mu_0} \sum_{m=1}^{M_1} \sum_{n=1}^{M_1} (k^2 - \tilde{k}_{4yn}^2) I_{6mn}^h \left\{ \frac{k_{4xm}}{k_{4xm} + \tilde{k}_{4xn}} \right\} A_{4m} \tilde{A}_{4n} - \\ &\quad \frac{k_z}{\omega \mu_0} \sum_{m=1}^{M_1} (k^2 - \tilde{k}_{4ym}^2) I_{5mm}^h \left\{ \frac{1}{2 \tilde{k}_{4xm}} \right\} \tilde{A}_{4m}^2 + \\ &\quad \frac{k_z}{\omega} \sum_{m=1}^{M_1} (k^2 - k_{4ym}^2) I_{2mm}^e \left\{ \frac{1}{2 k_{4xm}} \right\} A_{4m}^2 + \\ &\quad \frac{1}{\omega^2 \mu_0} \sum_{m=1}^{M_1} \sum_{n=1}^{M_1} (k^2 - k_{4yn}^2) I_{3nm}^e \left\{ \frac{\tilde{k}_{4xn}}{k_{4xm} + k_{4xn}} \right\} A_{4m} \tilde{A}_{4n} \end{aligned}$$

The total power in the device is equal to the sum of the powers calculated for each region of the line. It still remains, however, for the voltage across the strip to be calculated. In this case, the assumption is made that this voltage may be

approximated by the voltage at one point, the center point, of the strip. Thus, the voltage may be defined as:

$$V = - \int_0^{h_3} E_{2y} \Big|_{x=\frac{w_1+w_2}{2}} dy$$

where:

$$E_{2y} \Big|_{x=\frac{w_1+w_2}{2}, y} = \frac{1}{j\omega\epsilon(y)} \sum_{m=1}^{M_2} (k^2 - k_{2ym}^2) \psi_{2m}(y) \cdot \{A_{2m} \cos[k_{2xm}(w/2)] + B_{2m} \sin[k_{2xm}(w/2)]\}$$

Integrating from 0 to  $h_3$  yields:

$$V = - \frac{1}{j\omega} \sum_{m=1}^{M_2} (k^2 - k_{2ym}^2) \{A_{2m} \cos[k_{2xm}(w/2)] + B_{2m} \sin[k_{2xm}(w/2)]\} \cdot \left\{ \frac{A}{\epsilon_1} \sin[k_{2ym1}h_1] + \frac{B}{\epsilon_2} \sin[k_{2ym2}(h_2-h_1)] + \frac{C}{\epsilon_2 k_{2ym2}^2} \{1 - \cos[k_{2ym2}(h_2-h_1)]\} + \frac{D}{\epsilon_3} \cos[k_{2ym3}(h_3-h_2)] \right\}$$

where A, B, C, and D are the expansion coefficients defined in eqs. (2.2.6.a-2.2.6.d) for the TM<sup>y</sup> potential for the three-layer parallel-plate waveguide.

The current, I, on the strip is calculated from the transverse magnetic field on the strip. For a strip of zero thickness, the current I is given by:



$$\begin{aligned}
I &= \int_{\text{strip}} H_{\text{transverse}} \cdot ds = \\
&\int_{w_1}^{w_2} H_{2y}(y=h_3) \cdot dx + \int_{w_2}^{w_1} H_{3y}(y=h_3) \cdot dx = \\
&\sum_{m=1}^{M_2} \{j \cdot k_z \cdot d \cdot [(A_{2m} \cdot \sin(k_{2xm} \cdot w) + 2 \cdot B_{2m} \cdot \sin^2(k_{2xm} \cdot w/2)] + \\
&\quad \frac{1}{j \cdot \omega \cdot \mu_0} \tilde{d} \cdot [\tilde{A}_{2m} \cdot (1 - \cos(\tilde{k}_{2x} \cdot w)) - \tilde{B}_{2m} \cdot \sin(\tilde{k}_{2x} \cdot w)] - \\
&\sum_{m=1}^{M_3} \{j \cdot k_z \cdot \cos[k_{3ym} \cdot (h-h_3)] \cdot [A_{3m} \cdot \sin(k_{3xm} \cdot w) + \\
&\quad 2 \cdot B_{3m} \cdot \sin^2(k_{3xm} \cdot w/2) + \frac{1}{j \omega \mu_0} \cdot \cos[\tilde{k}_{3ym} \cdot (h-h_3)] \cdot \\
&\quad [\tilde{A}_{3m} \cdot (1 - \cos(\tilde{k}_{3xm} \cdot w)) - \tilde{B}_{3m} \cdot \sin(\tilde{k}_{3xm} \cdot w)]\}
\end{aligned}$$

The equations are now all in place to complete the analysis of the three-layered coupled microstrip line through the calculation of the propagation constant and the characteristic impedance of the line.

## Chapter 4. Numerical Results

The formulas derived for the calculation of the propagation constant and the characteristic impedance of the coupled microstrip line were implemented in Fortran 77. The Fortran program was run in double precision on the VAX or in single precision on the CRAY, with the same results. Some characteristic results are presented in this chapter.

### 4.1. Convergence Criteria

The exact electric and magnetic field representation for each region of the waveguide described in this thesis was given by an infinite sum of expansion functions, which were characteristic for each region of the device. Due to subsequent truncation of each infinite sum, the propagation constant which was derived for this structure was not exact, and the error present in the calculation not exactly known. However, as was presented in chapter 2, care was taken so that the relative number of expansion functions retained for each region was such that the truncation of the infinite series would lead to a convergent system. The accuracy of the results was determined via convergence plots, such as those shown in figs. (4.1.1) and (4.1.2). In these plots, the normalized propagation constant was plotted against the number of modes,  $M_2$ , retained in region 2 for the calculation of that particular value for the propagation constant. As  $M_2$  increases, the value of the normalized propagation constant converges to a particular value. So, after setting a certain error bracket as acceptable, the minimum  $M_2$  required to calculate the propagation constant within that error bracket is found from the convergence plots, and the corresponding normalized propagation constant is accepted as the solution.

This test cannot, however, be conducted for each data point, as the time taken to do this would be prohibitive. The procedure followed is to calculate the smallest  $M_2$  which satisfies the convergence conditions at the extreme data points. These points in this particular case would be smallest and largest structure size, and lowest and highest frequency. It is safe to accept that this  $M_2$  will then satisfy the same convergence criteria for any other point within the boundaries set by these extreme points.

The error bracket for the convergence plots are 0.5% for the propagation constant, and 1.5% for the characteristic impedance.

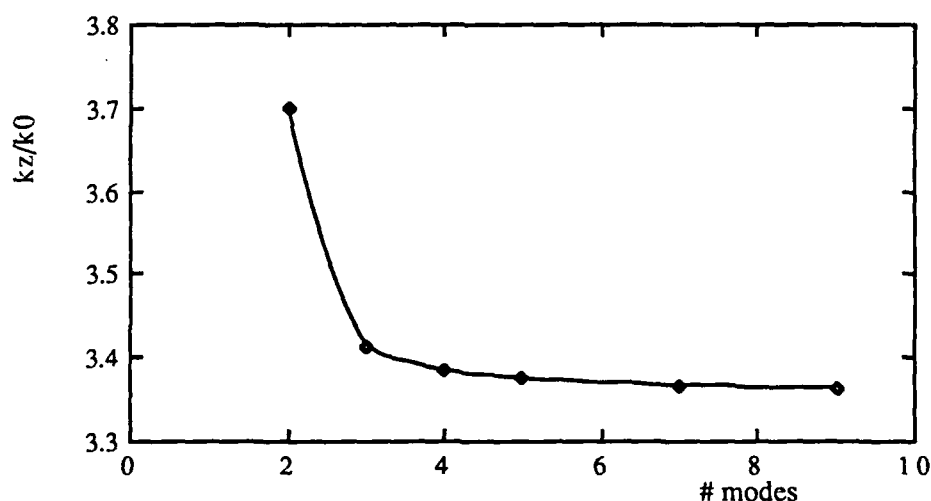


Figure 4.1.1. Convergence plot of the even mode propagation constant versus the number of modes retained in region 2.

Another important numerical consideration, which has been touched only briefly so far, is the height at which the top plate must be placed, such that it does not perturb the solution. It

was suggested in [19] that placing the top plate at a height double the height at which the metal strips are placed, would be enough to ensure an unperturbed solution. This is the height used for all the calculations. The same program was run for greater heights, but it was deduced that this only added unnecessarily to the computation time, without producing more accurate results.

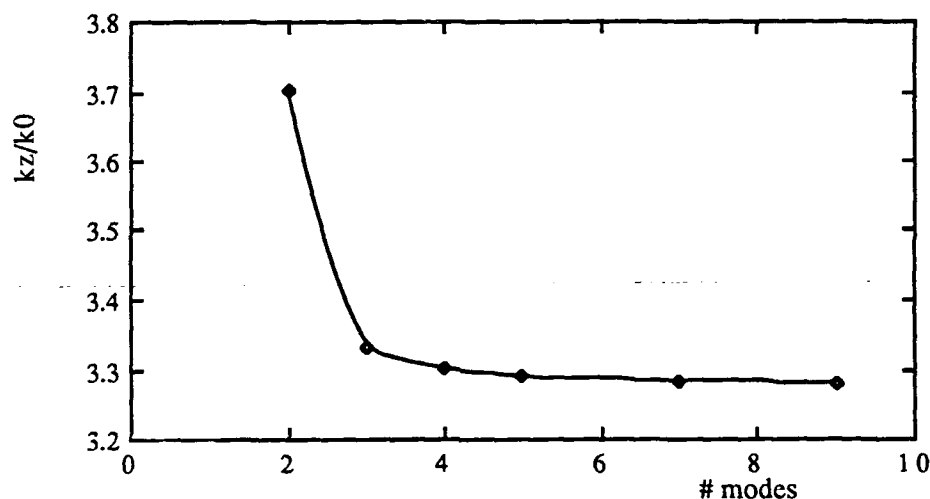


Figure 4.1.2. Convergence plot of the odd mode propagation constant versus the number of modes retained in region 2.

## 4.2. Program Verification

The accuracy of the programs was verified by selecting the permittivities of the dielectrics and the geometry of the structure such that it would be reduced to structures for which results were available. Both the propagation constant calculation and the characteristic impedance calculations for the single-layer, coupled microstrip line were verified against the results obtained by [2]. The calculation of the propagation constant for the single-line case was achieved by placing the striplines at a sufficiently large distance from each other. The results obtained for this case for the single-layer case were verified against [2], and for the multiple-layer case against [19 (p. 57)]. The calculation of the propagation constant for the three-layer coupled microstrip line was verified with [19 (p. 57)].

A comparison of the mode-matching technique versus the spectral-domain technique was achieved through the cooperation of Mr. Yu-De Lin, whose analysis may be found in [18]. The two different programs were run for the same coupled microstrip line, and the results are presented in the graphs in fig. 4.2.1. The results obtained from the mode matching method agree quite well with those obtained through application of the spectral-domain technique.

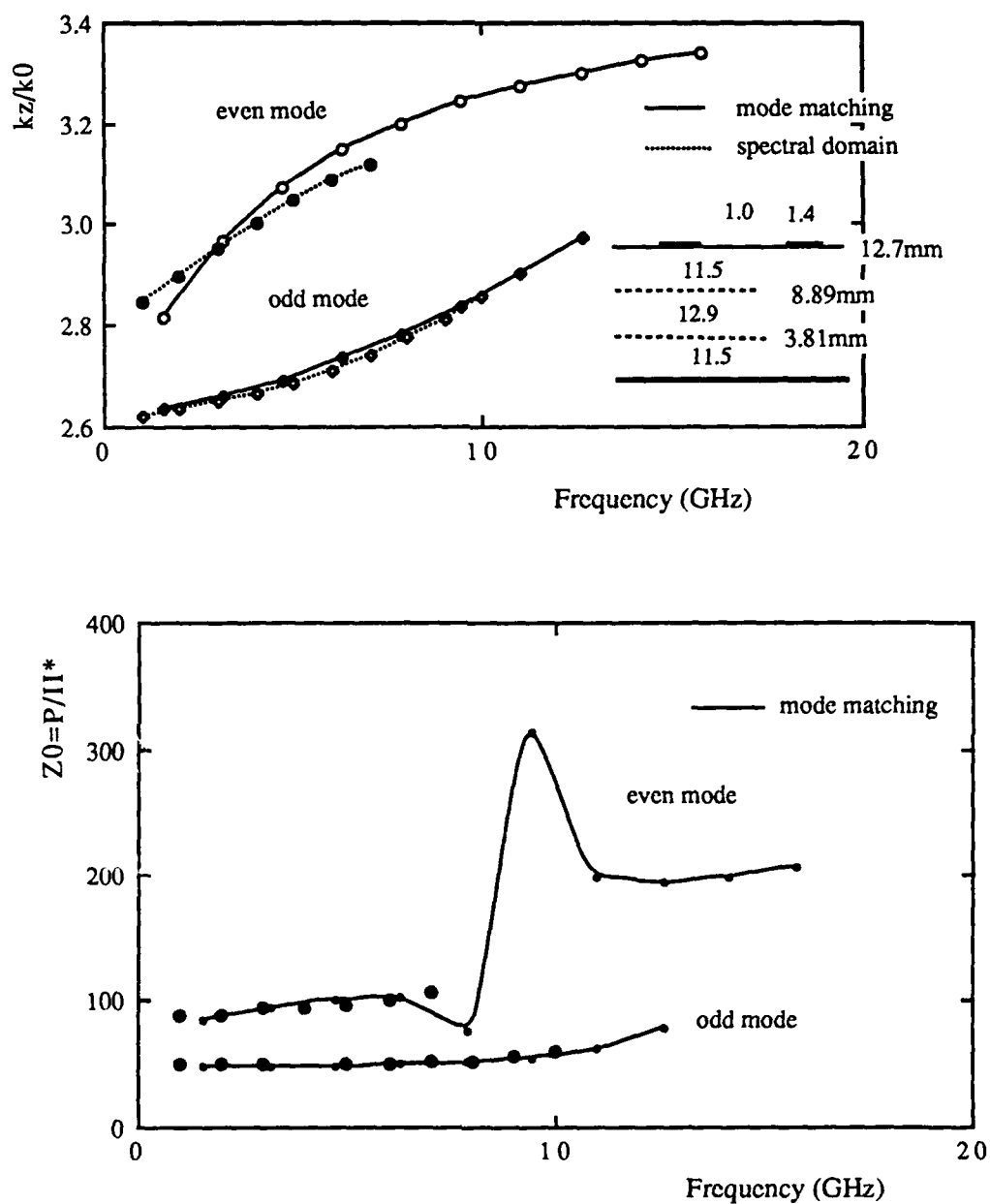


Figure 4.2.1. Propagation constant and characteristic impedance (power-current relationship) verification for the coupled microstrip line.

### 4.3. Results-Design Charts

The program was run for several cases of coupled microstrip lines. Each graph shows a family of curves, calculated for a specific microstrip width and dielectric layering, but for different strip separations, or for a variable dielectric constant in the conducting layer. In each case, for wider strip separation, the results converge to the case of a single microstrip line. Also, in the case of a variable dielectric constant value in the conducting layer, the results converge to the single-layer solution when the dielectric constant of the conducting layer approaches the value of the dielectric constant of the insulating layers.

Many curves were graphed versus a normalized frequency, where the normalization took the form  $2\pi h_3/\lambda_0$ , where  $\lambda_0$  is the free-space wavelength. The characteristic impedances, however, which are calculated using the power-voltage,  $Z_0 = V \cdot V^*/P$ , and the power-current,  $Z_0 = P/I \cdot I^*$ , expressions, exhibit discontinuities at regular intervals, which seem to correspond approximately to the frequency where  $h_3 = n\lambda_d/4$ , where  $n=1,2,3,\text{etc.}$ , and  $\lambda_d$  is the free-space wavelength in a medium of relative dielectric constant equal to the relative dielectric constants of the layered medium. This behavior is more evident where the characteristic impedance is plotted against  $h_3/\lambda_d$ . As the relative dielectric constant of the middle layer is increased with respect to the outer layers, this discontinuity becomes more pronounced, as may be witnessed in figs. 4.3.2(b), and (c). This behavior seems to signify the "turning on" of higher-order modes, which introduce a numerical instability around that region of frequencies. In figs. 4.3.6(b), and (c), the characteristic impedances are plotted over a wider range of normalized frequencies, and the almost "periodic" behavior of these discontinuities is more evident. The calculation of  $Z_0$  using  $Z_0 = V/I$  does not exhibit any discontinuous behavior.

4.3.1. Coupled microstrip line design charts for  $\epsilon_1=\epsilon_3=2.5$ ,  $\epsilon_2=3.9$ , and  $w=3.03\text{mm}$ .

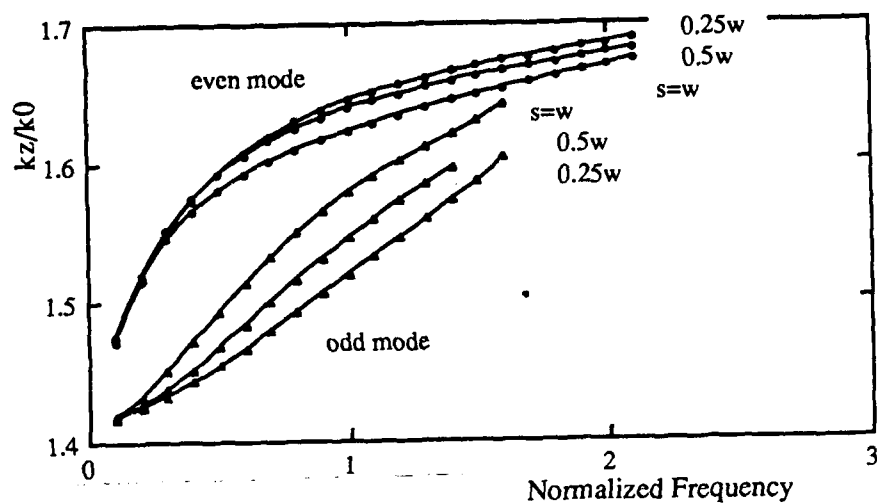


Figure 4.3.1(a).  $k_z/k_0$  versus  $2\pi h_3/\lambda_0$ .

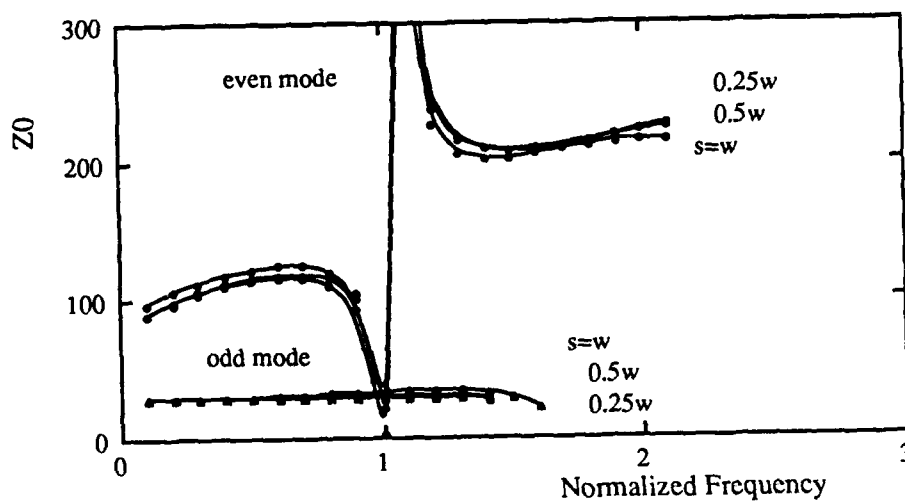


Figure 4.3.1(b).  $Z_0=P/I^*$  versus  $2\pi h_3/\lambda_0$ .



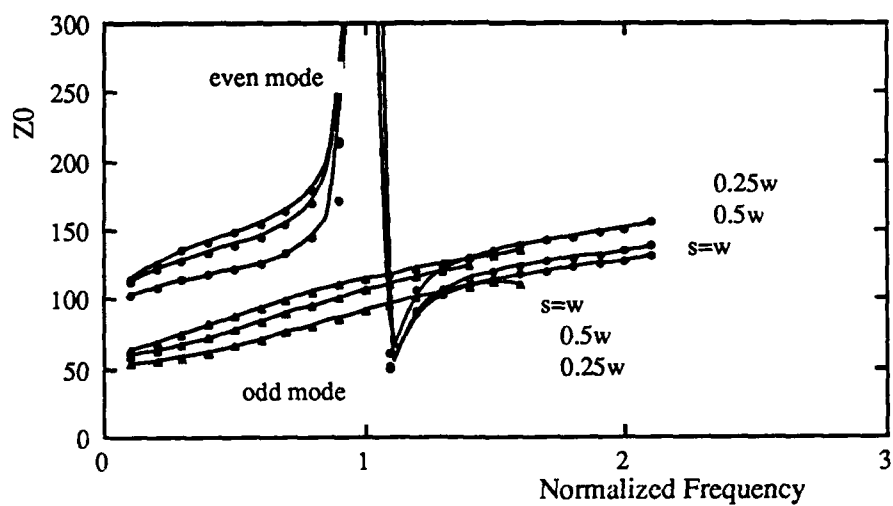


Figure 4.3.1(c).  $Z_0 = VV^*/P$  versus  $2\pi h_3/\lambda_0$ .

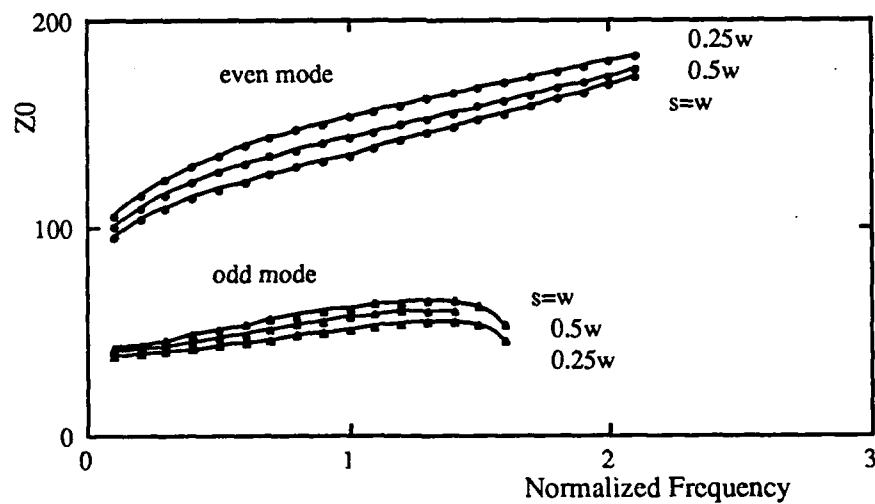


Figure 4.3.4.  $Z_0 = V/I$  versus  $2\pi h_3/\lambda_0$ .

4.3.2. Coupled microstrip line design charts for  $\epsilon_1 = \epsilon_3 = 10$ ,  $\epsilon_2 = 11, 12$ , and  $13$ , and  $w = 12.7\text{mm}$ .

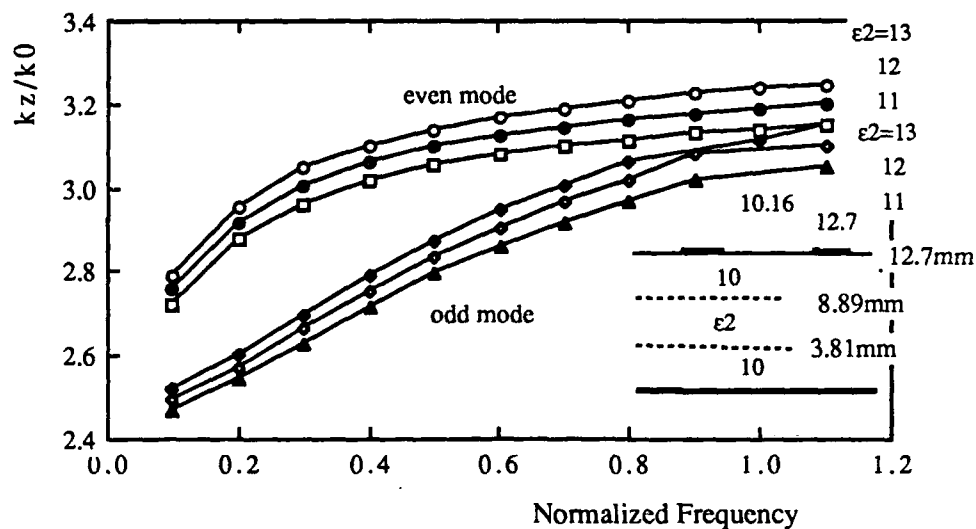


Figure 4.3.2(a).  $k_z/k_0$  versus  $2\pi h_3/\lambda_0$ .

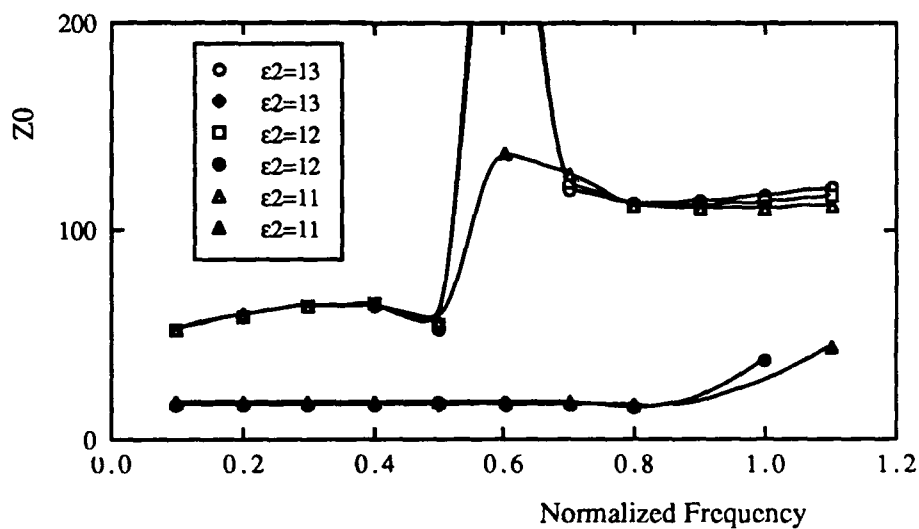


Figure 4.3.2(b).  $Z_0 = P/I^*$  versus  $2\pi h_3/\lambda_0$ .

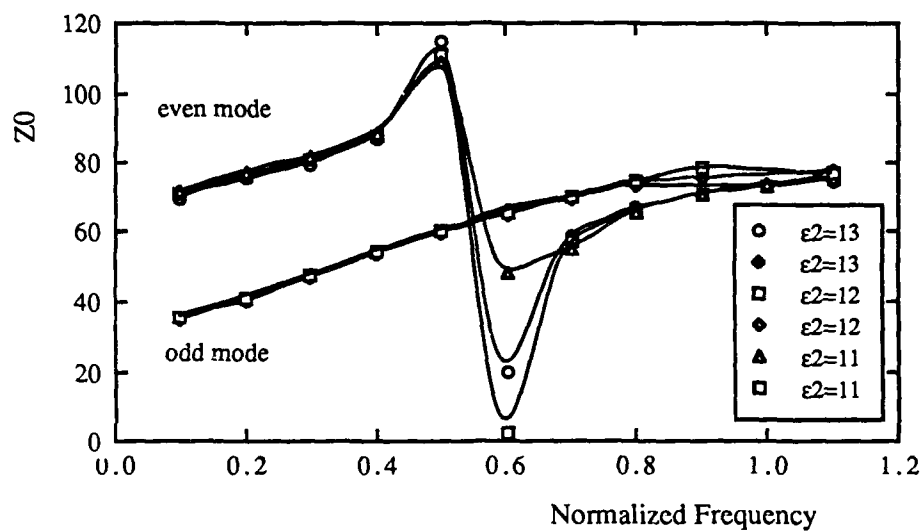


Figure 4.3.2(c)  $Z_0 = VV^*/P$  versus  $2\pi h_3/\lambda_0$ .

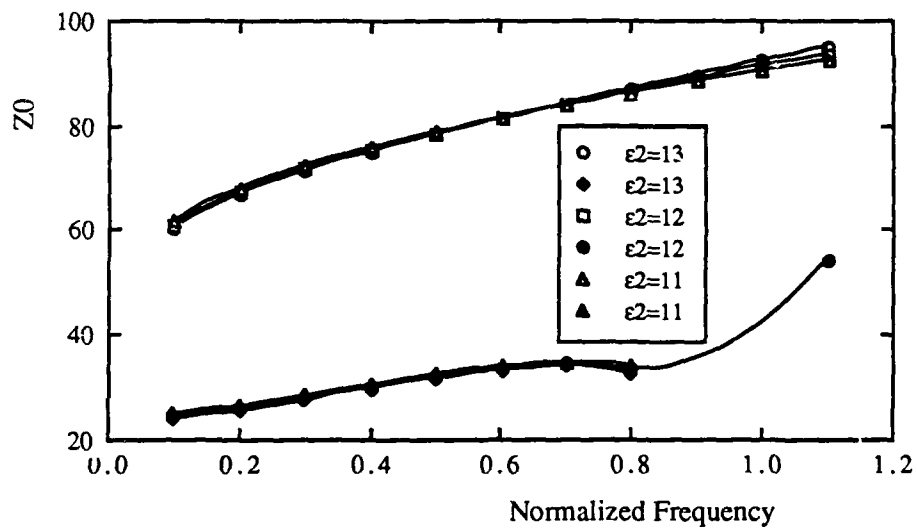


Figure 4.3.2(d)  $Z_0 = V/I$  versus  $2\pi h_3/\lambda_0$ .

**4.3.3. Coupled microstrip design charts for  $\epsilon_1=\epsilon_3=11.5$ ,  $\epsilon_2=12.9$ , and  $w=1.4\text{mm}$ .**

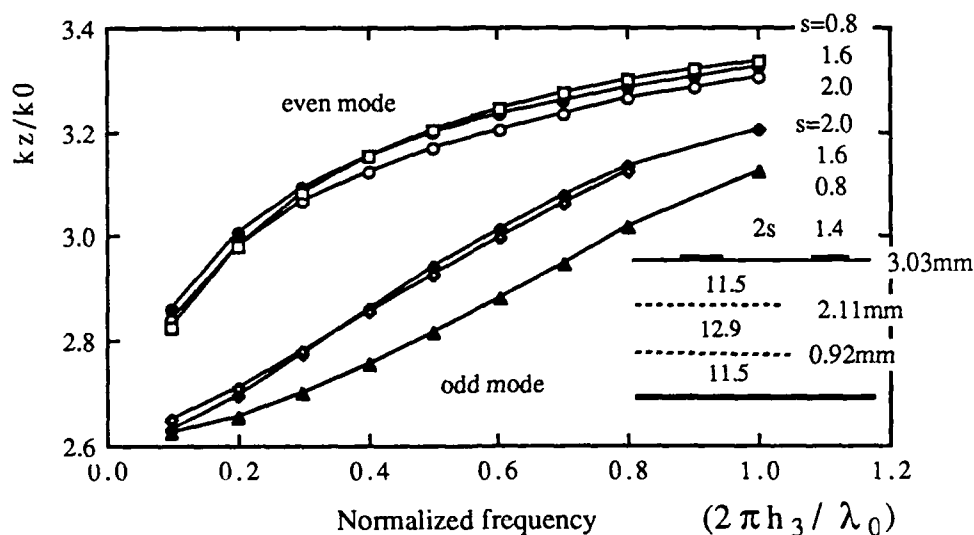


Figure 4.3.3(a).  $k_z/k_0$  versus  $2\pi h_3/\lambda_0$ .

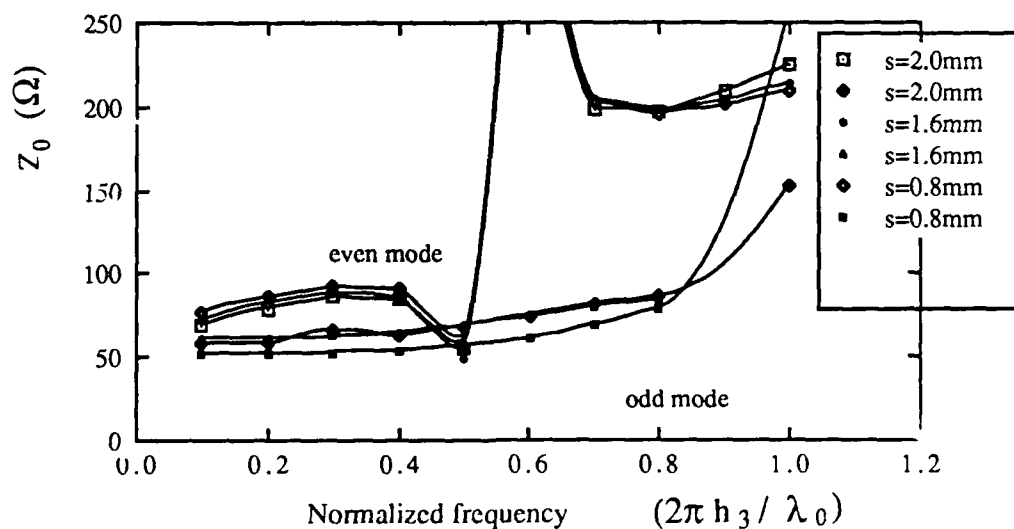


Figure 4.3.3(b).  $Z_0=P/I^*$  versus  $2\pi h_3/\lambda_0$ .

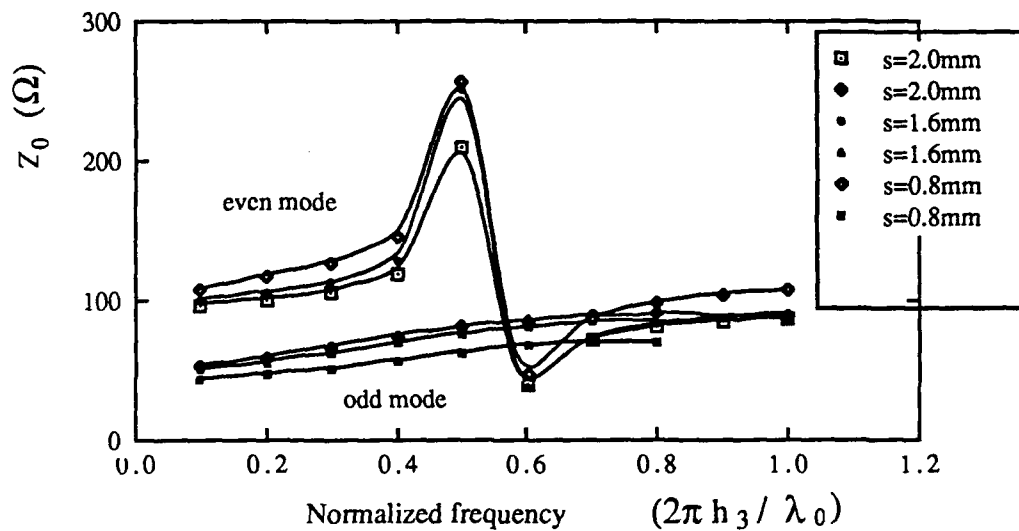


Figure 4.3.3(c).  $Z_0 = VV^*/P$  versus  $2\pi h_3 / \lambda_0$ .

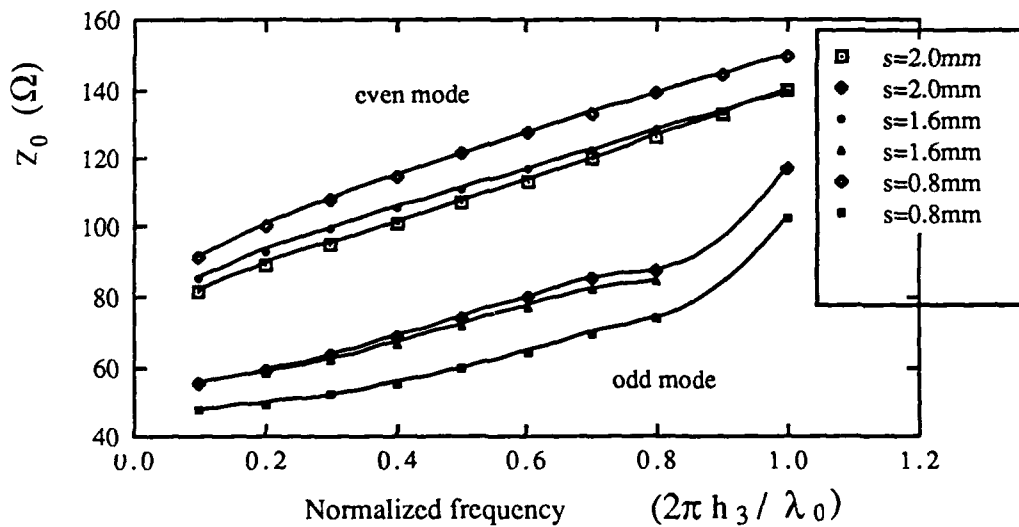


Figure 4.3.3(c).  $Z_0 = VV^*/P$  versus  $2\pi h_3 / \lambda_0$ .

**4.3.4. Coupled microstrip design charts for  $\epsilon_1=\epsilon_3=3.5$ ,  $\epsilon_2=4.9$ , and  $w=3.03\text{mm}$ .**

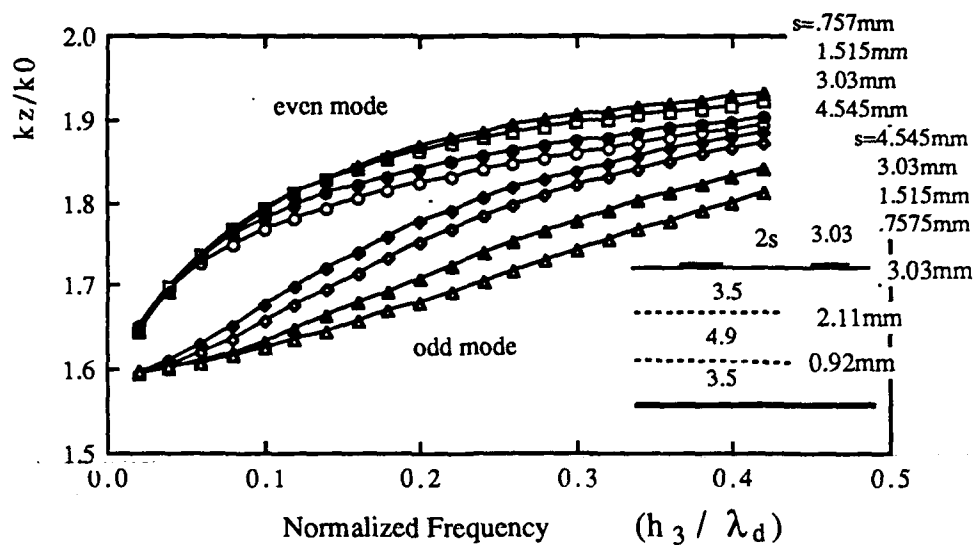


Figure 4.3.4(a).  $k_z/k_0$  versus  $h_3/\lambda_d$ .

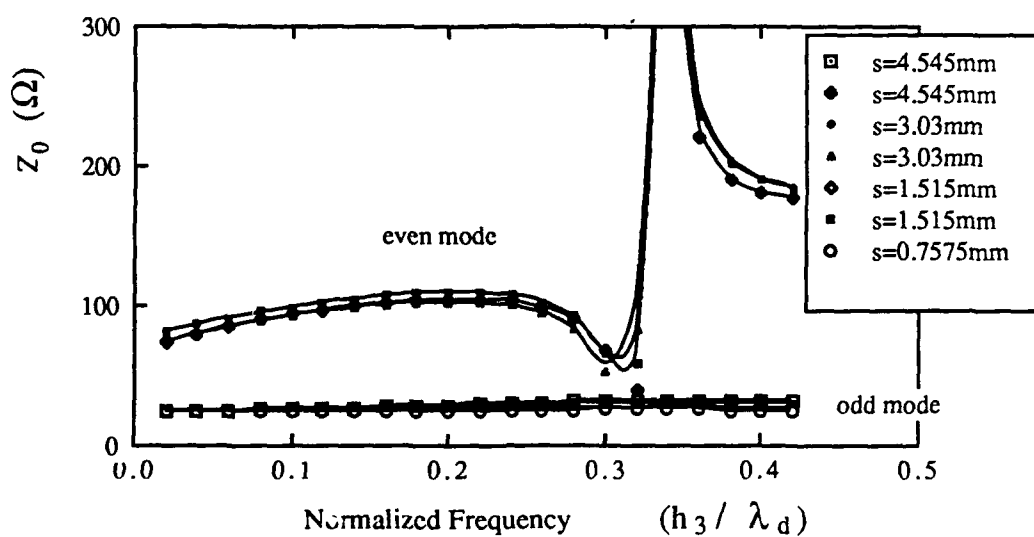


Figure 4.3.4(b).  $Z_0=P/I^*$  versus  $h_3/\lambda_d$ .

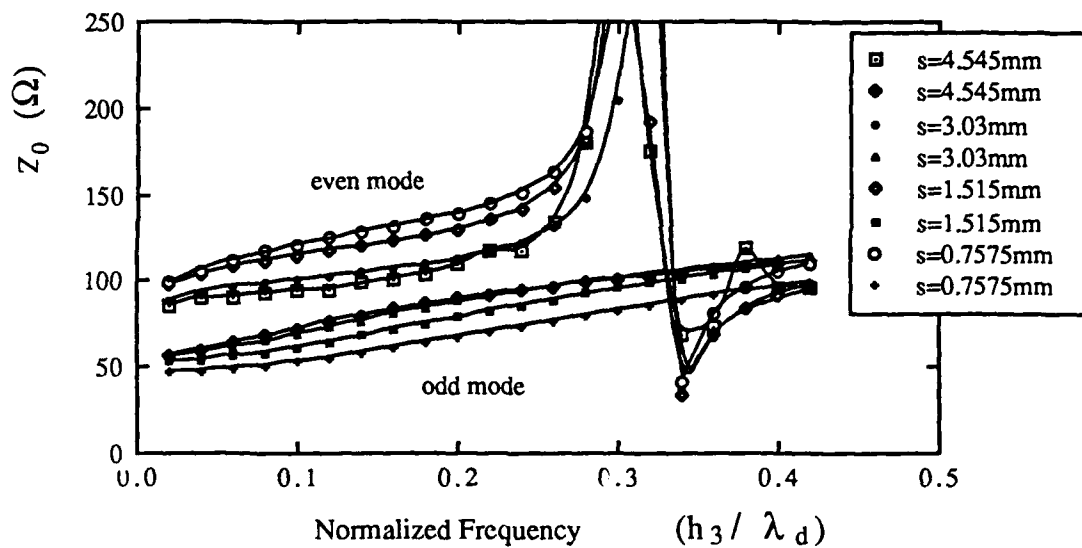


Figure 4.3.4(c).  $Z_0 = VV^*/P$  versus  $h_3/\lambda_d$ .

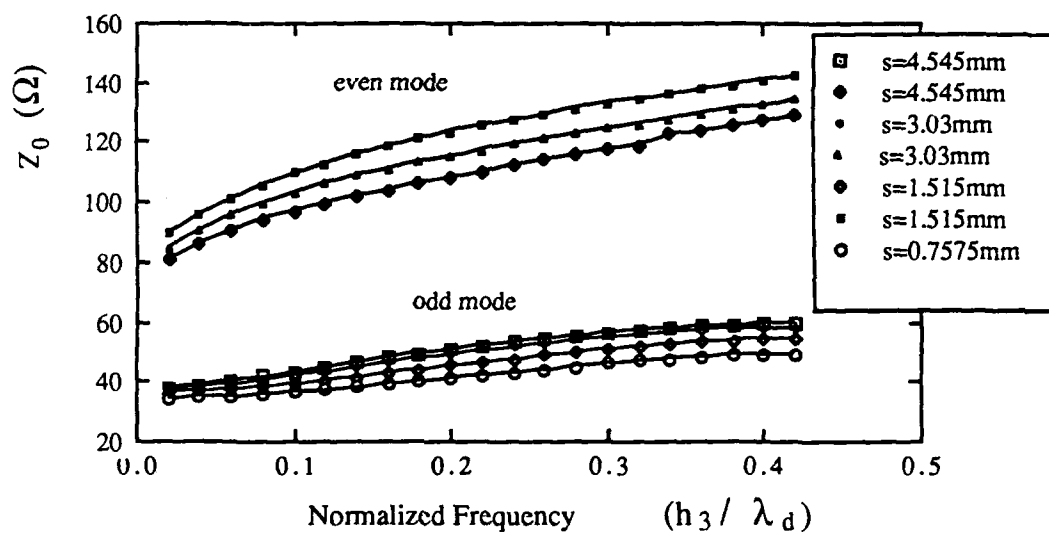


Figure 4.3.4(d).  $Z_0 = V/I$  versus  $h_3/\lambda_d$ .

**4.3.5. Coupled microstrip line design charts for  $\epsilon_1=\epsilon_3=3.5$ ,  $\epsilon_2=4.9$ ,  $w=1.4$ .**

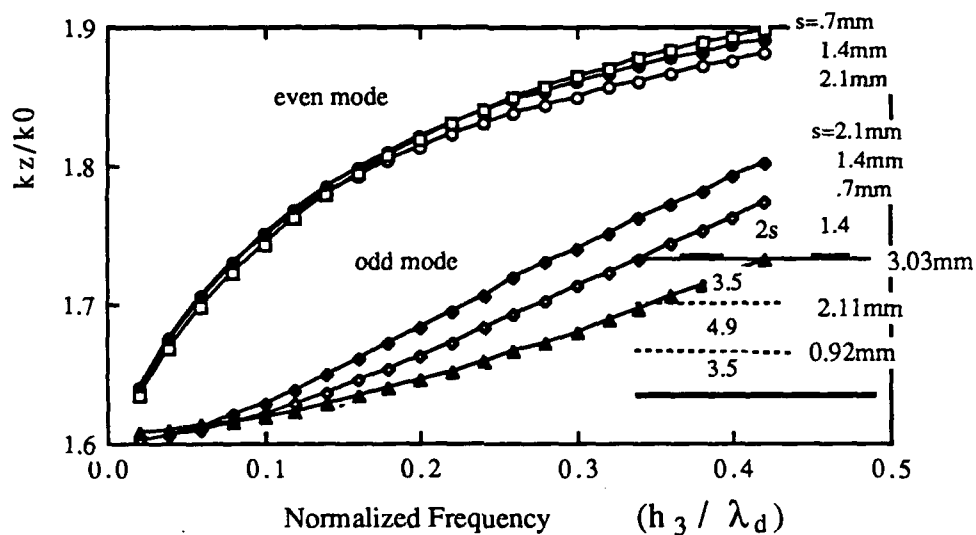


Figure 4.3.5(a).  $k_z/k_0$  versus  $h_3/\lambda_d$ .

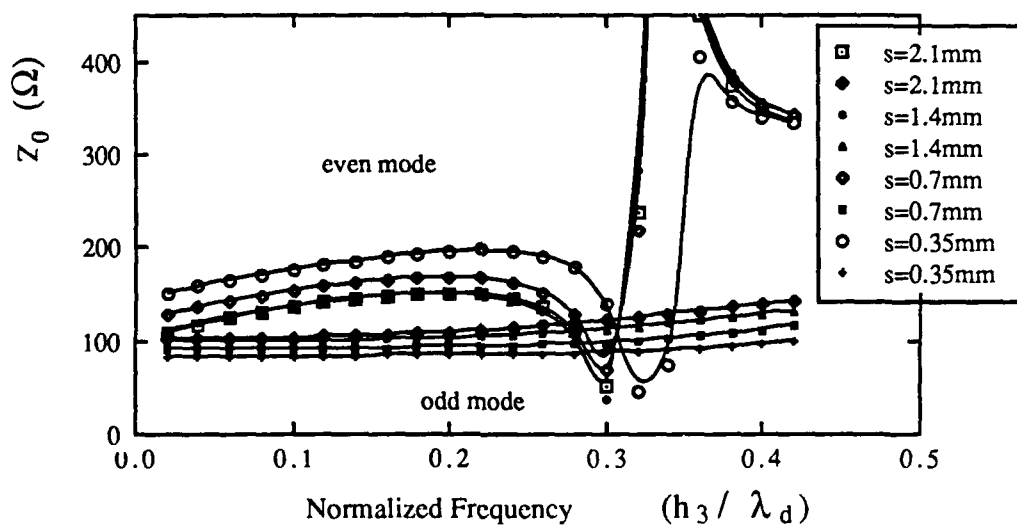


Figure 4.3.5(b).  $Z_0=P/\Pi^*$  versus  $h_3/\lambda_d$ .



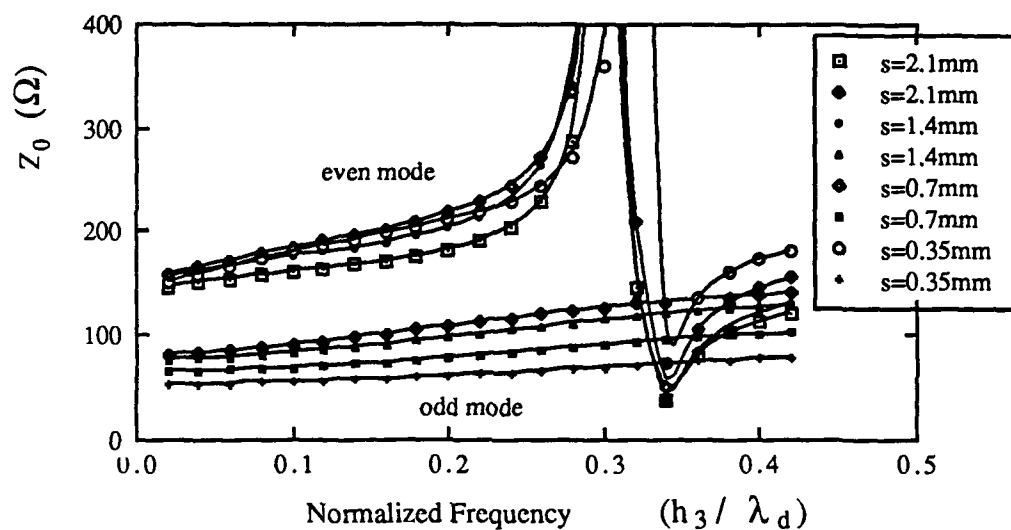


Figure 4.3.5(c).  $Z_0 = VV^*/P$  versus  $h_3/\lambda_d$ .

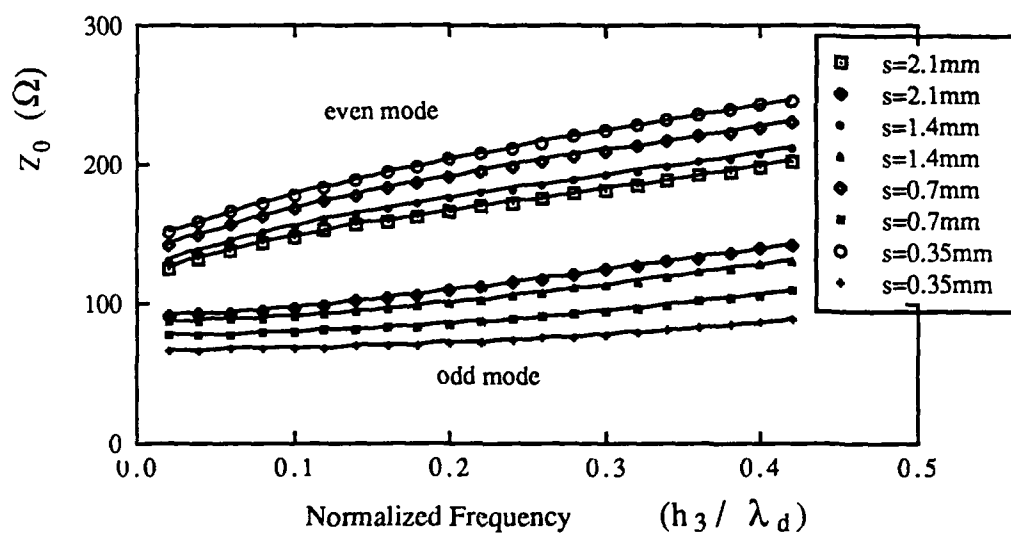


Figure 4.3.5(d).  $Z_0 = V/I$  versus  $h_3/\lambda_d$ .

**4.3.6. Observation of the behavior of the discontinuities in the characteristic impedance calculation over a wide range of frequencies.**

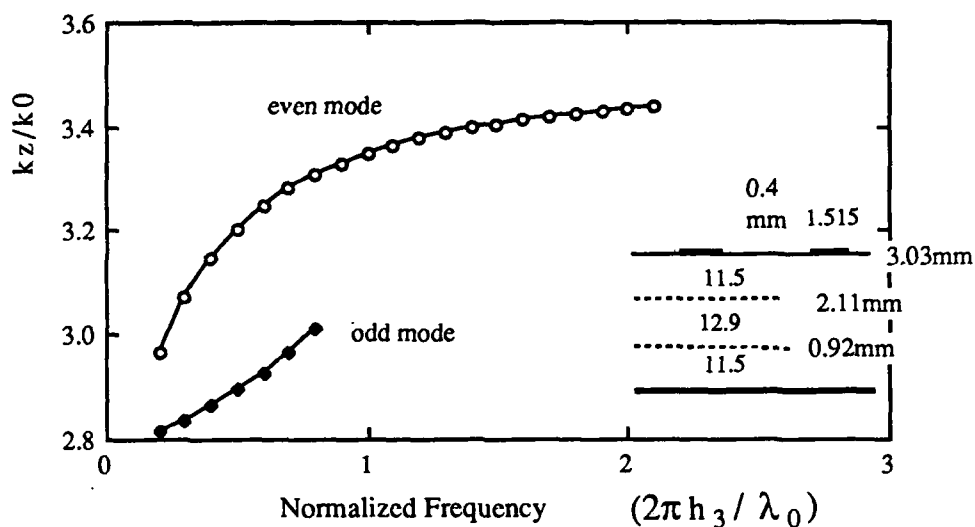


Figure 4.3.6(a).  $k_z/k_0$  versus  $2\pi h_3/\lambda_0$ .

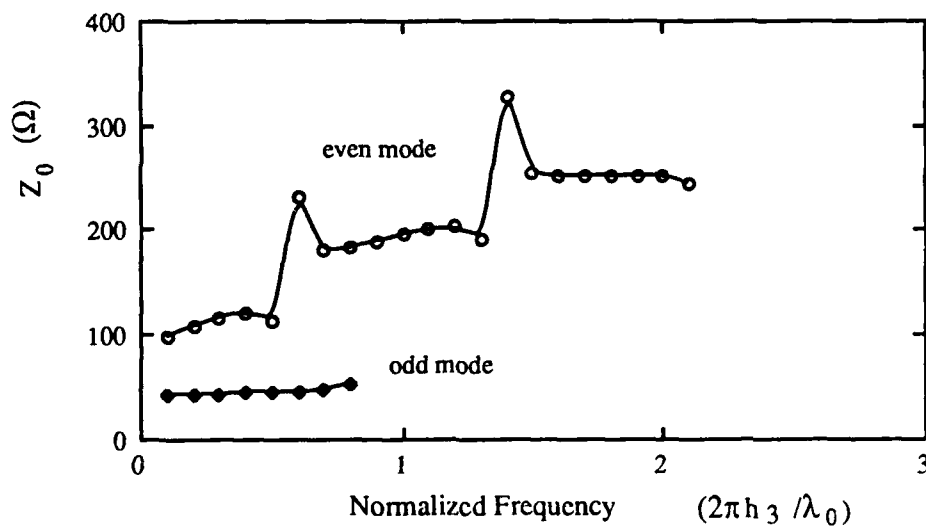


Figure 4.3.6(b).  $Z_0=P/I^*$  versus  $2\pi h_3/\lambda_0$ .

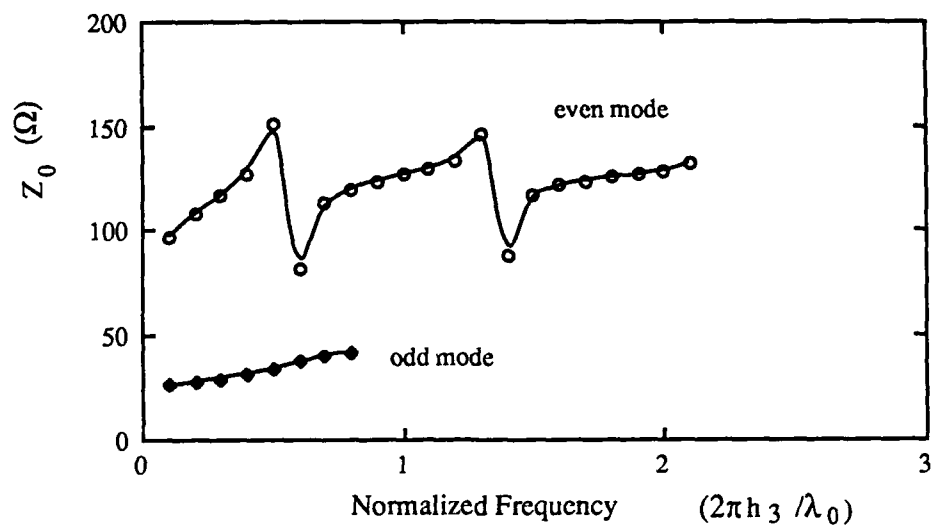


Figure 4.3.6(c).  $Z_0 = VV^*/P$  versus  $2\pi h_3/\lambda_0$ .

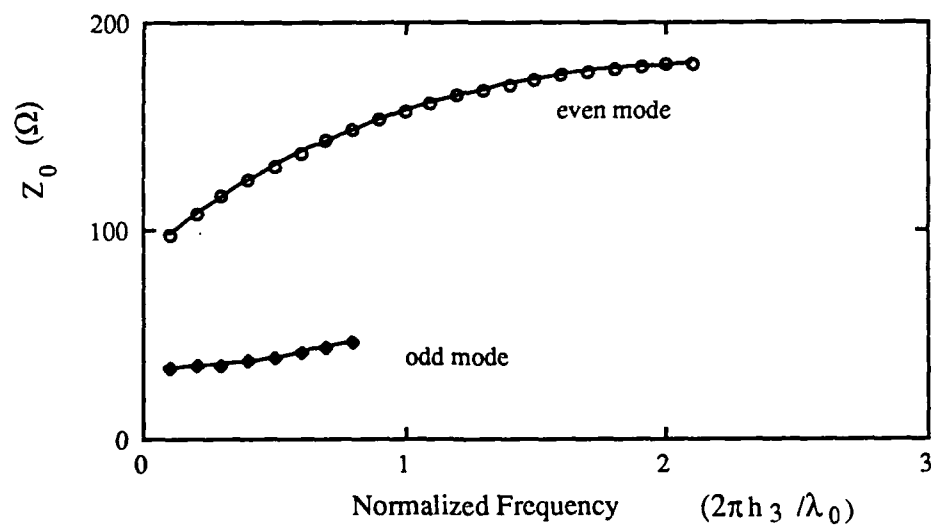


Figure 4.3.6(d).  $Z_0 = V/I$  versus  $2\pi h_3/\lambda_0$ .

## Chapter 5. Conclusions

In this thesis, it was shown how a quasi-planar structure like the coupled microstrip line on a layered dielectric substrate, could be analyzed using a variation of the mode matching technique.

Mode matching is a powerful tool for analyzing planar and even quasi-planar structures. The results obtained through mode matching have a high degree of accuracy, especially the propagation constant. This technique, however, is unsuitable for CAD packages, as it is very inefficient. It is also susceptible to numerical errors, as the system which is solved to calculate the field coefficients is defined by a singular matrix. It should be noted, as a matter of fact, that this singularity condition has actually been imposed on the matrix, in order to solve for the propagation constant.

The behavior of the even and odd mode propagation constants of the coupled microstrip line on a layered substrate does not differ from that of its single substrate counterpart, except for a slight increase of  $k_z/k_0$  with an increase in the conducting layer dielectric constant with respect to the insulating layer dielectric constants, as can be seen in fig. 4.3.2(a). As far as the impedance is concerned, it does not seem to change noticeably with the change in dielectric constants. The change becomes more noticeable, however, at higher frequencies. The effect of the discontinuity becomes much more noticeable for a higher conducting layer dielectric constant. Its position does not change much, however, as the values used for the dielectric constants were of the same order of magnitude.

The impedance curves seem to be relatively flat between singularities. The discontinuities themselves follow a

very consistent pattern which seems to be dictated by the relationship used to calculate the impedance (power-voltage, or power-current). Irrespective of the relationship used to calculate  $Z_0$ , however, the first singularity occurs at the same normalized frequency,  $h_3/\lambda_d \cong 0.25$ . This seems to be indicative of a cutoff frequency, above which higher order modes start propagating, and around which the calculations of the characteristic impedance become numerically unstable. It is not practical, in any case, to fabricate microstrip devices of the order of magnitude of  $\lambda_d/4$ , so only the portion of the curve before the discontinuity occurs is significant.

## Appendix A. Notation

A consistent notation scheme is used throughout the text where subscripts and superscripts are used to denote region, direction, dielectric, mode number, mode type, or to differentiate between two similar functions.

A variable "z" may take the form  $z_{abm}$  where "a" would be the cartesian coordinate (x, y, or z), "b" would be a region number (1, 2, 3, or 4), and "m" would be the mode number.

A function "f" may take the form  $f_{am}^{bc}$ , where "a" would be a function number, "m", and "n" would be mode numbers, and "c" would be the region number:  $c=2$  means the inner product was performed with respect to a normal mode of region 2, and  $c=3$  means the inner product was performed with respect to a normal mode of region 3. Superscript "b" is used only in the orthogonalization integrals:  $b=e$  means the inner product was performed with respect to a TM mode, and  $b=h$  means the inner product was performed with respect to a TE mode.

The following general notation was used to build the desired variables:

Symbol	Interpretation
$\epsilon$	permittivity
$\mu$	permeability
k	propagation constant
E	electric field
H	magnetic field

A tilde over any of the above variables would denote TE quantities, whereas no tilde would denote TM quantities.

## Appendix B. Derivation of Field Equations

A wave is a field that is a function of both time and space. Electric and magnetic fields that vary in time and space are governed by physical laws which are expressed in four equations, known as Maxwell's equations. For a wave travelling in a medium characterized by a certain permittivity,  $\epsilon$ , and a certain permeability,  $\mu$ , These equations are:

$$\nabla \times \mathbf{E} = -\mu \frac{\partial \mathbf{H}}{\partial t}$$

$$\nabla \times \mathbf{H} = \epsilon \frac{\partial \mathbf{D}}{\partial t} + \mathbf{J}$$

$$\nabla \cdot \mathbf{D} = \rho$$

$$\nabla \cdot \mathbf{B} = 0$$

(B.1)

The electromagnetic field equations above are expressed in terms of six quantities:

$\mathbf{E}$ , the electric intensity (in volts per meter)

$\mathbf{H}$ , the magnetic intensity (in amperes per meter)

$\mathbf{D}$ , the electric flux density (in coulombs per meter)

$\mathbf{B}$ , the magnetic flux density (in coulombs per square meter)

$\mathbf{J}$ , the electric current density (in amperes per square meter)

$\rho$ , the electric charge density (in coulombs per square meter)

The boldface script is used to denote complex quantities.

The ultimate sources of an electromagnetic field are the current  $\mathbf{J}$ , and the charge  $\rho$ .

The continuity equation, which is based on the principle of conservation of charge, is implicit in equations (B.1), and simply states that:

$$\nabla \cdot \mathbf{J} = -\frac{\partial \rho}{\partial t} \quad (\text{B.2})$$

Maxwell's equations are complemented by the so-called constitutive relationships, which incorporate the characteristics of the medium in which the field exists. These equations define the electric flux density,  $\mathbf{D}$ , the magnetic flux density,  $\mathbf{B}$ , and the current density,  $\mathbf{J}$ , with respect to the electric,  $\mathbf{E}$ , and magnetic,  $\mathbf{H}$ , intensities.

$$\begin{aligned} \mathbf{D} &= \mathbf{D}(\mathbf{E}, \mathbf{H}) \\ \mathbf{B} &= \mathbf{B}(\mathbf{E}, \mathbf{H}) \\ \mathbf{J} &= \mathbf{J}(\mathbf{E}, \mathbf{H}) \end{aligned} \quad (\text{B.3})$$

Maxwell's equations along with the constitutive relationships serve to fully describe a wave travelling in a known medium.

In a source free, linear medium, the constitutive relationships take the form:

$$\begin{aligned} \mathbf{D} &= \epsilon \mathbf{E} \\ \mathbf{B} &= \mu \mathbf{H} \\ \mathbf{J} &= 0 \end{aligned} \quad (\text{B.4})$$

Here,  $\epsilon$  and  $\mu$  are constants, where  $\epsilon$  is the capacitivity or permittivity, and  $\mu$  is the permeability of the medium. Using  $\epsilon_0$  and  $\mu_0$  to denote the corresponding variables in vacuum, for a perfect dielectric ( $\sigma=0$ ), one has  $\epsilon=\epsilon_r\epsilon_0$ , where  $\epsilon_r$  is the dielectric constant, or the relative capacitivity, of the medium, and  $\mu=\mu_0$  for most linear matter.



The present analysis will be concerned only with source free, linear problems, where the wave has a steady-state sinusoidal time dependence. In this case, the complex field equations read:

$$\begin{aligned} -\nabla \times \mathbf{E} &= \hat{z}(\omega) \mathbf{H} \\ \nabla \times \mathbf{H} &= \hat{y}(\omega) \mathbf{E} \\ \nabla \cdot \mathbf{D} &= 0 \\ \nabla \cdot \mathbf{B} &= 0 \end{aligned} \quad (\text{B.5})$$

where  $\hat{y}(\omega) = j\omega\epsilon$ , and  $\hat{z}(\omega) = j\omega\mu_0$  in nonmagnetic material.

The above representation of the field equations gives rise to the definition of the parameter  $k$ , the wavenumber of the medium. The wavenumber is defined as:

$$k = \sqrt{-\hat{y}(\omega) \hat{z}(\omega)} \quad (\text{B.6})$$

The physical meaning of the wavenumber is that  $1/k$  is the velocity of propagation of an electromagnetic disturbance in an open space filled with perfect dielectric material with permittivity  $\epsilon$  and permeability  $\mu_0$ .

Taking the curl of equations (B.5), and using the above representation of  $k$ , the complex wave equations become:

$$\begin{aligned} \nabla \times \nabla \times \mathbf{E} - k^2 \mathbf{E} &= 0 \\ \nabla \times \nabla \times \mathbf{H} - k^2 \mathbf{H} &= 0 \end{aligned} \quad (\text{B.7})$$

In these equations, it is implicit that:

$$\nabla \cdot \mathbf{E} = 0 \quad \text{and} \quad \nabla \cdot \mathbf{H} = 0 \quad (\text{B.8})$$

so that a simplified form for the vector wave equations may be derived:

$$\nabla^2 \mathbf{E} + k^2 \mathbf{E} = 0 \quad (\text{B.9})$$

and:

$$\nabla^2 \mathbf{H} + k^2 \mathbf{H} = 0 \quad (\text{B.10})$$

The geometry of planar structures allows us to work with rectangular cartesian coordinates. In this case, the rectangular components of  $\mathbf{E}$  and  $\mathbf{H}$  satisfy the complex scalar wave equation:

$$\begin{aligned} \nabla^2 E_i + k^2 E_i &= 0 \\ i &= x, y, z \\ \nabla^2 H_i + k^2 H_i &= 0 \end{aligned} \quad (\text{B.11})$$

To construct a pliable solution to the above equations, the field is expressed as a magnetic vector potential  $\mathbf{A}$  and an electric vector potential  $\mathbf{F}$ , as shown below:

$$\begin{aligned} \mathbf{E} &= -\nabla \times \mathbf{F} + \frac{1}{y} \nabla \times \nabla \times \mathbf{A} \\ \mathbf{H} &= \nabla \times \mathbf{A} + \frac{1}{z} \nabla \times \nabla \times \mathbf{F} \end{aligned} \quad (\text{B.12})$$

These expressions for  $\mathbf{E}$  and  $\mathbf{H}$  give rise to a very useful classification of the solutions of the wave equation. In this classification, axial uniformity (the cross-sectional shapes of the waveguide do not vary in the direction of propagation) is assumed. In addition, this classification is for fields conforming to the homogeneous vector Helmholtz equations (source free

problem). Propagation is assumed to be in the  $z$  direction, and the  $z$  dependence is assumed to be of the form  $\exp(\pm j\beta z)$ . The Helmholtz equation is separable, so a solution of scalar Helmholtz equation of the form  $f(z)g(x,y)$  is sought.

Under this classification, the vector magnetic and electric potentials,  $A$  and  $F$  respectively, may be assumed to be directed along one coordinate only.

Choosing  $A = u_x \psi$  where  $\psi$  is a scalar wave potential (a solution of the scalar Helmholtz equation), will yield an electromagnetic field given by:

$$\begin{aligned} E_x &= \frac{1}{\hat{y}} \left( \frac{\partial^2}{\partial x^2} + k^2 \right) \psi & H_x &= 0 \\ E_y &= \frac{1}{\hat{y}} \frac{\partial^2 \psi}{\partial x \partial y} & H_y &= \frac{\partial \psi}{\partial z} \\ E_z &= \frac{1}{\hat{y}} \frac{\partial^2 \psi}{\partial x \partial z} & H_z &= - \frac{\partial \psi}{\partial y} \end{aligned} \quad (B.13)$$

This choice of a magnetic vector potential will yield Transverse Electric to  $x$  ( $TE^x$ ) modes. The main characteristic of these modes is that  $E_z=0$  and  $H_z \neq 0$ . All  $TE^x$  field components may be derived from the axial component  $H_z$  of the magnetic field. All field components may be derived from the axial component  $H_z$  of the magnetic field.

Similarly, choosing  $F = u_x \psi$  will yield an electromagnetic field given by :

$$\begin{aligned}
 \tilde{E}_x &= 0 & \tilde{H}_x &= \frac{1}{z} \left( \frac{\partial^2}{\partial x^2} + k^2 \right) \tilde{\psi} \\
 \tilde{E}_y &= -\frac{\partial \tilde{\psi}}{\partial z} & \tilde{H}_y &= \frac{1}{z} \frac{\partial^2 \tilde{\psi}}{\partial x \partial y} \\
 \tilde{E}_z &= \frac{\partial \tilde{\psi}}{\partial y} & \tilde{H}_z &= \frac{1}{z} \frac{\partial^2 \tilde{\psi}}{\partial x \partial z}
 \end{aligned}
 \tag{B.14}$$

This choice of an electric vector potential will yield Transverse Magnetic to x (TM<sup>x</sup>) or E modes. The main characteristics of these modes are that :

$$\tilde{E}_z \neq 0 \text{ and } \tilde{H}_z = 0 \tag{B.15}$$

All TM<sup>x</sup> field components may be derived from the axial component  $H_z$  of the magnetic field.

The third group in this classification are the TEM modes, or the transverse electromagnetic waves. The waves belonging to this classification have no  $E_z$  or  $H_z$  component. In this case, the electric field may be found from the gradient of a scalar function  $\psi(x,y)$ , which is a function of the transverse components only, and is a solution of the two-dimensional Laplace equation. True TEM waves, however, will be found to occur in very few cases (i.e., free-space, parallel-plate waveguide, etc.). In addition, true TE and TM modes will usually not be sufficient to satisfy all the boundary conditions of most structures. In such cases, however, linear combinations of TE and TM modes will provide a complete and general solution.

As might be anticipated, TE<sup>x</sup> and TM<sup>x</sup> are not the only existing TE and TM solutions to a specific problem. By assuming

the magnetic vector potential to have the form  $\mathbf{A} = \mathbf{u}_y \psi$ , the following equations for the fields will be derived:

$$\begin{aligned} E_x &= \frac{1}{y} \frac{\partial^2 \psi}{\partial x \partial y} & H_x &= -\frac{\partial \psi}{\partial z} \\ E_y &= \frac{1}{y} \left( \frac{\partial^2}{\partial x^2} + k^2 \right) \psi & H_y &= 0 \\ E_z &= \frac{1}{y} \frac{\partial^2 \psi}{\partial y \partial z} & H_z &= \frac{\partial \psi}{\partial x} \end{aligned} \quad (\text{B.16})$$

This choice of  $\mathbf{A}$  will yield Transverse Electric to  $y$  ( $\text{TE}^y$ ) modes, whose main characteristics are that  $E_y \neq 0$  and  $H_y = 0$ .

Similarly, taking  $\mathbf{F} = \mathbf{u}_y \psi$  will yield:

$$\begin{aligned} \tilde{E}_x &= \frac{\partial \tilde{\psi}}{\partial z} & \tilde{H}_x &= \frac{1}{z} \frac{\partial^2 \tilde{\psi}}{\partial x \partial y} \\ \tilde{E}_y &= 0 & \tilde{H}_y &= \frac{1}{z} \left( \frac{\partial^2}{\partial x^2} + k^2 \right) \tilde{\psi} \\ \tilde{E}_z &= -\frac{\partial \tilde{\psi}}{\partial z} & \tilde{H}_z &= \frac{1}{z} \frac{\partial^2 \tilde{\psi}}{\partial y \partial z} \end{aligned} \quad (\text{B.18})$$

This choice of electric vector potential will yield Transverse Magnetic to  $y$  ( $\text{TM}^y$ ) modes, whose main characteristics are that  $E_y = 0$  and  $H_y \neq 0$ .

Similar cases may be derived for  $\text{TE}^z$  and  $\text{TM}^z$ .

## References

- [1] Herbert J. Carlin, and Pier P. Civalleri, "A Coupled-Line Model for Dispersion in Parallel-Coupled Microstrips", IEEE Trans. Microwave Theory Tech., pp.444-446, May 1975.
- [2] Jeffrey B. Knorr, and Ahmet Tufekcioglou, "Spectral-Domain Calculation of Microstrip Characteristic Impedance", IEEE Trans. Microwave Theory Tech., vol. MTT-23, no.9, pp.725-728, September 1975.
- [3] E. Yamashuti, and K. Atsuki, "Analysis of Microstrip-Like Transmission Lines by Nonuniform Discretization of Integral Equations", IEEE Trans. Microwave Theory Tech., vol. MTT-24, no.4, pp.195-200, April 1976.
- [4] Klaus Solbach, and Ingo Wolff, "The Electromagnetic Fields and the Phase Constants of Dielectric Image Lines", IEEE Trans. Microwave Theory Tech., vol. MTT-26, no.4, pp.266-275, April 1978.
- [5] D. Mirshikar-Syahkal, and Brian Davies, "Accurate Solution of Microstrip and Coplanar Structures for Dispersion and for Dielectric and Conductor Losses", IEEE Trans. Microwave Theory Tech., vol. MTT-27, no.7, pp.694-699, July 1979.
- [6] Arne Brejning Dalby, "Interdigital Microstrip Circuit Parameters Using Empirical Formulas and Simplified Model", IEEE Trans. Microwave Theory Tech., vol. MTT-27, no.8, pp.744-752, August 1979.
- [8] Raj Mittra, Yun-Li Hou, and Vahraz Jamnejad, "Analysis of Open Dielectric Waveguides Using Mode-Matching Technique and Variational Methods", IEEE Trans. Microwave Theory Tech., vol. MTT-28, no.1, pp.36-43, January 1980.

[9] S.-J. Peng, and A. A. Oliner, "Guidance and Leakage Properties of a Class of Open Dielectric Waveguides: Part I-Mathematical Formulations", IEEE Trans. Microwave Theory Tech., vol. MTT-29, no.9, pp.843-854, September 1981.

[10] Ulrich Crombach, "Analysis of Single and Coupled Rectangular Dielectric Waveguides", IEEE Trans. Microwave Theory Tech., vol. MTT-29, no.9, pp.870-874, September 1981.

[11] Yoshiro Fukuoka, Yi-Chi Shih, and Tatsuo Itoh, "Analysis of Slow-Wave Coplanar Waveguide for Monolithic Integrated Circuits", IEEE Trans. Microwave Theory Tech., vol. MTT-31, no.7, pp.567-573, July 1983.

[12] J. R. Brews, "Characteristic Impedance of Microstrip Lines", IEEE Trans. Microwave Theory Tech., vol. MTT-35, no.1, pp.30-34, January 1987.

[13] R. F. Harrington, "Time-Harmonic Electromagnetic Fields", New York, McGraw-Hill, 1961.

[14] R. E. Collin, "Foundations for Microwave Engineering", New York, McGraw-Hill, 1966.

[15] R. Mittra, and S. W. Lee, "Analytic Techniques in the Theory of Guided Waves", New York, Macmillan, 1971.

[16] S. J. Leon, "Linear Algebra with Applications", New York, Macmillan, 1980.

[17] S. Ramo, J. Whinnery, and J. Van Duzer, "Fields and Waves in Communications Electronics", New York, John Wiley and Sons, 1984.

[18] Yu-De Lin, "Metal-Insulator-Semiconductor Coupled Microstrip Lines", Master's Thesis, University of Texas, Austin, TX, 1987.

[19] Brian Young, "Analysis and design of Microslab Waveguide", Dissertation, University of Texas, Austin, TX, 1987.